

Cite this: *Org. Biomol. Chem.*, 2024, **22**, 7460

Synthesis of C-glycoside analogues of isopropyl β -D-1-thiogalactopyranoside (IPTG) and 1- β -D-galactopyranosyl-2-methylpropane. Conformational analysis and evaluation as inhibitors of the lac repressor in *E. coli* and as galactosidase inhibitors†

Eoin Hever,^a Venkatesan Santhanam,^b  Sherivan Alberi,^a Ashis Dhara,^a 
Mikael Bols,^b  Heinz-Peter Nasheuer^a and Paul V. Murphy^{a,c} *

Isopropyl 1-thio- β -D-galactopyranoside (IPTG, **1**) is used widely as an inducer of protein expression in *E. coli* and 1- β -D-galactopyranosyl-2-methylpropane (**2**), a C-glycoside analogue of **1**, has also been identified as an inducer. Here, synthesis and study of mimetics of **1** and **2**, 1- β -D-galactopyranosyl-2-methylpropan-1-ols and two cyclic acetals derivatives, that constrain the presentation of the iPr group in various geometries is described. Conformational analysis of C-glycosides in protic solvent is performed using (i) Desmond metadynamics simulations (OPLS4) and (ii) use of $^3J_{\text{HH}}$ values obtained by $^1\text{H-NMR}$ spectroscopy. 1- β -D-Galactopyranosyl-2-methylpropane (**2**) is an effective protein expression inducer when compared to the new mimetics, which were less effective or did not induce expression. 1- β -D-Galactopyranosyl-2-methylpropane (**2**) led to significantly reduced proteolysis during protein expression, compared to IPTG suggesting that recombinant protein purification will be easier to achieve with **2**, yielding proteins with higher quality and activity. IPTG reduced bacterial growth to a greater degree than **2** compared to the control. IPTG's isopropyl group was observed by molecular dynamics (MD) simulations to be flexible in the binding pocket, deviating from its crystal structure binding mode, without impacting other interactions. The MD simulations predicted that 1- β -D-galactopyranosyl-2-methylpropane (**2**) was more likely than IPTG to bind the repressor with a conformation favoured in protic solvent, while maintaining interactions observed for IPTG. MD simulations predicted that isobutanol derivatives may disrupt interactions associated with IPTG's binding mode. The compounds were also evaluated as inhibitors of galactosidases, with **2** being the more potent inhibitor of the *E. coli* β -galactosidase. The constrained cyclic acetals showed similar inhibition constants to IPTG indicating *E. coli* β -galactosidase can recognize galactopyranoses with varying presentation of the iPr group.

Received 2nd August 2024,
Accepted 20th August 2024

DOI: 10.1039/d4ob01286k

rsc.li/obc

1. Introduction

The S- and C-glycosides¹ are mimetics of O-glycosides, which are of interest due to their stability to hydrolysis that occurs under acidic conditions or in the presence of enzymes and accordingly have potential as therapeutic agents or as tools where chemically and biochemically stable glycomimetics are needed. Conformational preferences of C-glycosides² and S-glycosides³ are relevant as they may influence affinity and selectivity for carbohydrate binding receptors.⁴ Another feature of C-glycosides is that the glycosidic carbon can be substituted more than oxygen, enabling additional interactions with receptors to be facilitated, or which can alter conformation preference around the C-C bond.

^aSchool of Biological and Chemical Sciences, University of Galway, University Road, Galway, Ireland, H91TK33. E-mail: paul.v.murphy@universityofgalway.ie

^bDepartment of Chemistry, Københavns Universitet, Universitetsparken 5, 2100 København Ø, Denmark

^cSSPC – the Science Foundation Ireland Research Centre for Pharmaceuticals, University of Galway, University Road, Galway, Ireland, H91TK33

†Electronic supplementary information (ESI) available: Additional experimental procedures and analytical data; ^1H and ^{13}C NMR spectra of 1–6 and intermediates; geometry after protein preparation of IPTG bound to lac repressor; MD simulations analysis for compounds 1, 2, 4 and 5 with the lac repressor. See DOI: <https://doi.org/10.1039/d4ob01286k>



Many saccharides, such as galactopyranosides/gluco-pyranosides adopt chair structures for the pyranose ring (4C_1). For disaccharides, such as lactose (Gal β 1-4Glc), the glycosidic torsion preferences, for ϕ and Ψ , are the main influence on disaccharide conformation. The *exo*-anomeric effect influences conformation preference about the C–O (glycoside) bond and steric and torsional strain are also factors. For *C*-glycosides, there is no *exo*-anomeric effect⁵ and conformational preference for the C–C bond is primarily governed by minimization of steric and torsional strain. Staggered conformations are generally preferred for the ϕ and Ψ torsions in *C*-glycosides, as reported by Kishi *et al.*⁶ and by Barbero *et al.*⁷ In contrast an eclipsed conformation can be preferred for Ψ in *O*-disaccharides like lactose.

Applications of *S*- and *C*-glycosides include lectin inhibitors,⁸ as decoy substrates for bacterial glycosyltransferases⁹ or as glycoprocessing inhibitors.¹⁰ The topic herein relates to the influence of isopropyl thio- β -D-galactopyranoside (IPTG, **1**) and its *C*-glycoside mimetics on the *Escherichia coli* (*E. coli*) lac promoter/repressor.¹¹ Components of the *E. coli* lac operon, and hybrid promoters containing the lac operator sequence such as TAC and T5-lac promoters, have been modified to enable expression of recombinant proteins, which is in wide use. Allolactose (Gal β 1,6Glc), formed *in situ* from lactose (Gal β 1,4Glc), binds to the lac repressor¹² and induces a conformational change, that greatly reduces affinity of the repressor for DNA, facilitating protein translation. β -Galactosidase, produced after induction of protein expression, hydrolyses the glycosidic bond present in lactose/allolactose, removing the inducer and thereby allowing the repressor to inhibit protein synthesis. On the other hand, IPTG is a stable mimetic of allolactose, and is not hydrolysed by β -galactosidase, and, thus, is widely used for induction of the lac operon. IPTG induces a conformational change in the repressor, allosterically inhibiting repressor binding to DNA, and enabling protein synthesis. As it is stable to β -galactosidase, the concentration of the IPTG is believed to remain constant and protein synthesis is not inhibited.

Various small molecule inducers of protein expression have been investigated.¹³ IPTG (**1**) was identified as a high affinity binder to the lac repressor, with affinity similar to the natural inducer allolactose, and \sim 100 fold higher affinity than its *O*-glycoside counterpart, isopropyl β -D-galactopyranoside (IPG), which is also an inducer. Being an inducer is associated with binding the repressor and a corresponding low affinity of the repressor for DNA. Anti-inducers were also identified, which show affinity for the repressor but these substances interact to increase affinity between the repressor and DNA. Thirdly, nitrophenyl β -D-galactopyranoside (ONPG) is a non-inducer, capable of binding to the repressor, but not influencing its interaction with DNA. Unlike ONPG, nitrophenyl-1-thio- β -D-galactopyranoside (T-ONPG), the *S*-glycoside mimetic, is a potent inducer and it was speculated by Lewis and co-workers that this could be due to flexibility of the *S*-glycoside compared to the *O*-glycoside. The crystal structure of IPTG **1** at 2 Å resolution indicated that the galactopyranoside's 6-OH is involved in

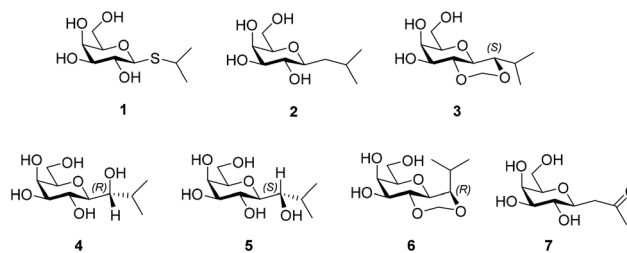


Chart 1 Chemdraw structures of 1–7.

stabilizing interactions between the repressor's Ser193 and Asp149, which is believed to induce an inactive conformation of the repressor.¹⁴

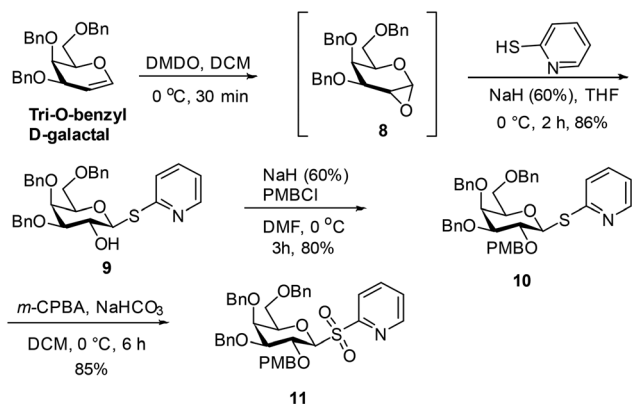
The *C*-glycosyl compound, 1-(β -D-galactopyranosyl)-2-methyl-propane (**2**)¹⁵ was earlier shown by Pohl and co-workers to have similar or improved induction properties compared to IPTG.¹⁶ Increased ligand preorganization into a bioactive conformation can reduce the entropic penalty when binding, which is in turn reflected in an affinity increase, and so, ligand conformational preorganization may be important.¹⁷ Here, we synthesised of analogues of **2** (isobutanols) with a hydroxyl substituent at the anomeric carbon, such as **4** & **5**, and also prepared **3** and **6** to probe the role of increasing conformation restriction; we evaluated how these *C*-glycosides compared to **1** and **2**, in inhibiting (i) the lac repressor and (ii) inhibiting galactosidases, to provide biological context for the research.¹⁸ We included **7** for the induction experiments. We did find an advantage in using **2** compared to **1** in protein expression in that there was reduced proteolysis of the expressed protein, which may be an indicator of reduced stress. While the newly synthesised *C*-glycosides did not induce or only weakly induced protein synthesis, they did show comparable activity as inhibitors of β -galactosidase compared to IPTG (Chart 1). We performed conformational analysis of **1**–**6** and computational methods were used to investigate interaction of ligands to the lac repressor in attempt to rationalize results.

2. Results and discussion

2.1 Synthesis of 1–7

Several methods exist for *C*-glycoside synthesis and this topic has been comprehensively reviewed.¹⁹ Samarium iodide (SmI₂) promoted *C*-glycoside synthesis was used in this work.²⁰ Thus, the synthesis started with preparation of a glycosylsulfone **11** from tri-*O*-benzyl- β -galactal, which underwent epoxidation using dimethyldioxirane generated *in situ*²¹ to afford **8**. The epoxide **8**²² is sensitive to hydrolysis and, avoiding chromatographic purification, was subjected to nucleophilic reaction with 2-mercaptopyridine in presence of sodium hydride to give β -substituted thioglycoside **9** in 86% yield. Reaction of **9** with *p*-methoxybenzyl chloride in presence of sodium hydride (60% in mineral oil) gave the PMB ether **10** (80%), which on sub-



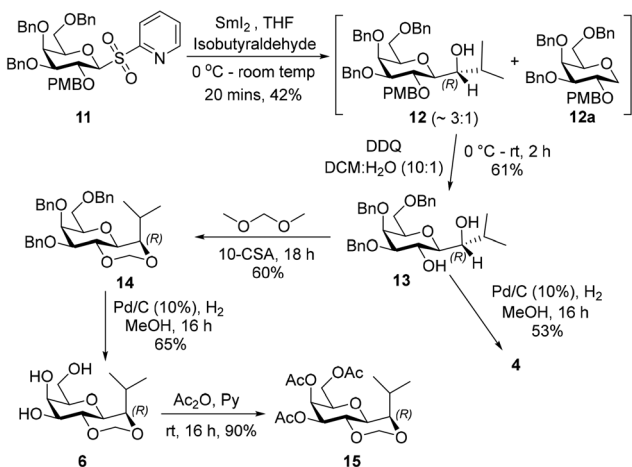


Scheme 1 Preparation of the sulfone 11.

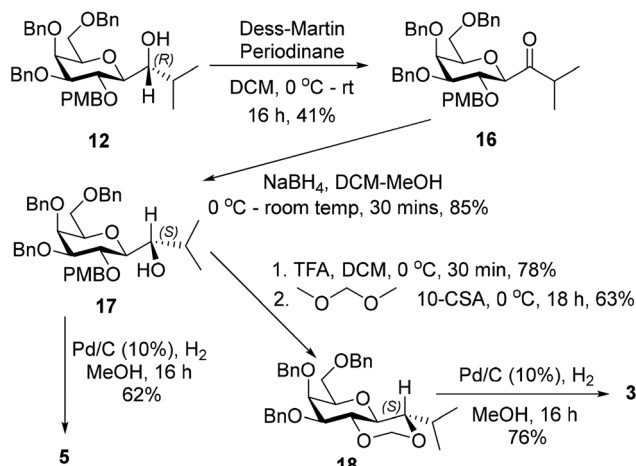
sequent oxidation by *m*-chloroperoxybenzoic acid gave sulfone 11 in 85% yield (Scheme 1).

The reaction of a freshly prepared SmI_2^{23} with sulfone 11 in the presence of isobutyraldehyde gave the secondary alcohol 12 in 42% yield. The NMR spectral analysis indicated that the presence of the 1-deoxygalactopyranose 12a as an impurity from reaction of 11, which was inseparable from the product (ratio 12a : 12 = ~1 : 3). Removal of the PMB ether from the mixture of 12 and 12a using 2,3-dichloro-5,6-dicyano-1,4-benzoquinone (DDQ)²⁴ followed by chromatography led to isolation of diol 13 in 61% yield. Debencylation of 13 by catalytic hydrogenation in the presence of 10% Pd-C gave 4 in 53% yield. Treatment of 13 with dimethoxymethane in the presence of camphorsulfonic acid²⁵ provided the acetal 14 in 60% yield. Debencylation of 14 afforded 6 in 65% yield. Debencylation of 14 by catalytic hydrogenation in the presence of 10% Pd-C to afford 6 in 65% yield (Scheme 2).

Product 6 was peracetylated, to give 15, which enabled stereochemical configuration determination as ¹H-NMR spectrum of 15 showed reduced signal overlap compared to 6. The ¹H-NMR spectrum of 15 displayed a ³J value of 5.7 Hz for the coupling between the galactopyranosyl H-1 (δ 3.68 ppm) and



Scheme 2 Synthesis of 4 and 6.



Scheme 3 Synthesis of 3 & 5.

the isopropyl group H (δ 3.72 ppm), which is consistent with H-1 being axial and the isopropyl H being equatorial in the acetal containing ring. This implied the configuration of each of the intermediates 12–14 and of products 4 and 6 at the carbon indicated in Scheme 2 is (*R*).

The (*S*)-diastereoisomer, 17, was obtained (85%) in a two-step oxidation reduction sequence, after treating alcohol 12 with Dess–Martin periodinane, followed by reduction of the resulting ketone with sodium borohydride. Removal of the PMB group from 17 using trifluoroacetic acid afforded the expected diol in 78% yield which was further treated with dimethoxymethane in the presence of CSA to give 18 in 63% yield. Debencylation of 18 afforded 3 in 76% yield. Debencylation of 17 by catalytic hydrogenation in the presence of 10% Pd-C gave 5 in 62% yield (Scheme 3).

Compound 2 was synthesized according to the 3-step procedure previously reported by Pohl *et al.* (see Scheme S1†). Compound 7 was also prepared as described previously.²⁶

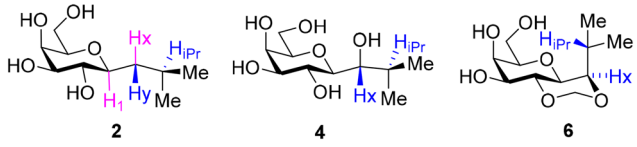
2.2 Conformational analysis of 1–6

2.2.1 Conformational analysis using ³J values obtained by ¹H-NMR spectroscopy.

For 1–6 the NMR spectroscopic data, recorded in CD₃OD, shows that the pyranose rings have the expected ⁴C₁ (*i.e.* the chair with most substituents equatorial) and that the main conformational differences between 1–6 is likely to be in the orientation of the *i*Pr group, which can be defined by preferences of two torsions: (i) ϕ , the dihedral angle defined by atoms H1–C1–X–C_{*i*Pr}, where X = S or C and C_{*i*Pr} is the methanetriyl carbon; (ii) ψ , the dihedral angle defined by C1–X–C_{*i*Pr}–H_{*i*Pr}, where H_{*i*Pr} is the hydrogen atom bonded to the methanetriyl carbon. The ¹H-NMR spectra give ³J_{HH} values in CD₃OD which give an indication whether the two relevant protons prefer the antiperiplanar arrangement (*i.e.* $\phi = +gauche$; $\psi = +gauche$) on adjacent carbon atoms (Table 1), which is associated with ³J_{HH} values >8.0 Hz based on the Karplus equation.²⁷ For 2, the ³J_{HH} values (see Table 1) measured in D₂O were essentially identical with those



Table 1 Selected $^3J_{\text{HH}}$ values (Hz) measured in CD_3OD unless otherwise stated: antiperiplanar C–H bonds are highlighted in purple or blue



Compd	$^3J_{\text{H1, HX}}$	$^3J_{\text{H1, HY}}$	$^3J_{\text{HX, HiPr}}$	$^3J_{\text{HY, HiPr}}$
2	10.0	2.1	4.2	9.7
2 (D_2O)	9.9	2.1	4.3	9.9
3	9.1	—	2.8	—
4 (<i>R</i>)	1.6	—	8.7	—
5 (<i>S</i>)	5.2	—	5.2	—
6	n.d.	—	10.0	—
15	5.7	—	10.3	—

measured in CD_3OD , indicating the same conformation is preferred in the two protic solvents. While eclipsing (synperiplanar) C–H bonds cannot be ruled out based on the observed J values, molecular modelling calculations did not indicate such eclipsing conformers are low in energy for *C*-glycosides and the earlier work of Kishi and Barbero and co-workers indicate that *C*-glycosides have staggered conformations. Thus, we propose that 2 and 4 adopt preferentially the $\phi = +gauche$; $\psi = +gauche$ conformer in protic solvent based on the $^3J_{\text{HH}}$ values.

2.2.2 Coordinate scanning and metadynamics. Low energy minimum conformational isomers were generated for 1–6 using (i) coordinate scanning in MacroModel²⁸ (using GBSA water model & OPLS4 force field²⁹), and (ii) metadynamics simulations using Desmond³⁰ (using OPLS4 force field in SP3 water box), with both methods implemented in Maestro.³¹ For the metadynamics the current variables (CVs) selected were the ϕ and ψ dihedral angles as defined above. The conformational preferences for the *S*- and *C*-glycosides were benchmarked against IPG using the molecular mechanics methods. Unlike the *S*- and *C*-glycoside, the conformation of IPG is influenced by the *exo*-anomeric effect as well as steric and torsional strain, with the ϕ angle defined by atoms H1–C1–O–C_{iPr} (see Fig. 1) for the lowest energy conformer +49° (*exo-syn* or +*gauche*). The *exo-syn* conformer is lower in energy than *exo-anti*, due to the additional *gauche* repulsive interaction between the isopropyl group and the galactopyranose axial H-2, analogous to a *gauche* interaction in butane; it is also lower in energy than the non-*exo* conformer. The ψ -angle is defined by the C1–O–C_{iPr}–H_{iPr} atoms and indicates the conformational preference about the O–C_{iPr} bond a preference for a staggered arrangement where $\psi = +40^\circ$ (+*gauche*); a second conformer with $\phi = \textit{exo-syn}$ and $\psi = \sim -60^\circ$ (–*gauche*) is ~ 1 kcal mol^{–1} higher in energy.

The energy plots obtained from metadynamics for 1–6, with water as solvent are shown in Fig. 2 and geometries for the lowest energy conformer are displayed in Fig. 3. The metadynamics was performed in CH_3OH also for 1–6, as this was the solvent used for NMR, with the same lowest energy conformer and similar energy surfaces found as in water. For IPTG 1,

the $\phi = +gauche$ and $\psi = +gauche$ conformer was lowest in energy, like that found in its crystal structure.³² Other low energy conformers identified from the metadynamics simulation had ϕ and ψ angles approximating to those of 1a, 1b, 1d and 1e found by DFT. Metadynamics of 2 showed a preference for the $\phi = +gauche$ and $\psi = +gauche$ conformation which is consistent with the $^3J_{\text{HH}}$ values measured experimentally. For 4 the $\phi = +gauche$ and $\psi = +gauche$ is preferred based on the metadynamics and this is also supported by the $^3J_{\text{HH}}$ values. For 5, in the metadynamics simulations, the anti-conformer, like in 5c, was lowest in energy, not 5a as predicted by DFT in the gas phase, most likely due to intramolecular H-bonding being disrupted by interaction with solvent³³ and this conformer geometry agrees with $^3J_{\text{HH}}$ values measured. Metadynamics predicted the $\phi = +gauche$ for 3 and $\phi = \textit{anti}$ for 6, due to the cyclic acetal constraint; the ¹H-NMR data show that the pyranose rings adopt ⁴C₁ geometry in 3 and 6. Thus 3 is a highly constrained mimetic of the preferred $\phi = \textit{exo-syn}$ conformation of the *O*-glycoside. For 6 the $^3J_{\text{HH}}$ value of 10.0 Hz observed in the isopropyl CH signal, assigned to the coupling between this proton and the adjacent acetal ring proton, is consistent with the low energy conformer found for 6 by metadynamics (Fig. 3).

2.3 Induction of protein expression in *E. coli* and growth by glycomimetic compounds

To determine the activity of glycomimetics in the induction of recombinant proteins in *E. coli*, the expression of monomeric teal fluorescent protein 1 (mTFP1) was investigated following standard procedures.³⁴ In brief, bacterial cells BL21(DE3) harboring the vector pQLinkHD-mTFP1 were treated with 1 mM of compounds. At the indicated times, bacterial culture samples were collected and OD₆₀₀ values were determined with a colorimeter 45 (ThermoFisher Scientific). Additionally, mTFP1 expression levels were measured with an Applied Biosystems StepOnePlus™ PCR System (ThermoFisher) by determining fluorescence in the blue channel. To this end, bacterial culture material, $V = 30 \mu\text{l}$, was centrifuged at 13 500 rpm for 5 min at 4 °C. The supernatant was removed, and the cell pellets were suspended in 90 μl of phosphate-buffered saline yielding a 1/3 dilution of the cell concentration and frozen at –20 °C until fluorescence measurement was ready to be taken. After thawing of the cell suspension, 20 μl of the cell suspension were transferred into Applied Biosystems MicroAmp™ 96-Well Reaction plates (ThermoFisher Scientific) for measuring the amount of fluorescence at 25 °C in the blue channel of an Applied Biosystems StepOnePlus™ quantitative PCR System (ThermoFisher Scientific). Then the fluorescence value for the samples were normalized to the OD₆₀₀ value and the highest value of the 24 h time point was arbitrarily set to 1.

Additionally, the mTFP1 expression was investigated by western blotting. At the indicated times, 500 μl of bacteria cultures were collected and centrifuged. The cell pellets were suspended in 50 μl of PBS (yielding a 10-fold concentration). For SDS PAGE, 5 μl of a culture with 1 OD₆₀₀ was loaded on a 10% SDS polyacrylamide gel (loading volumes were adjusted to



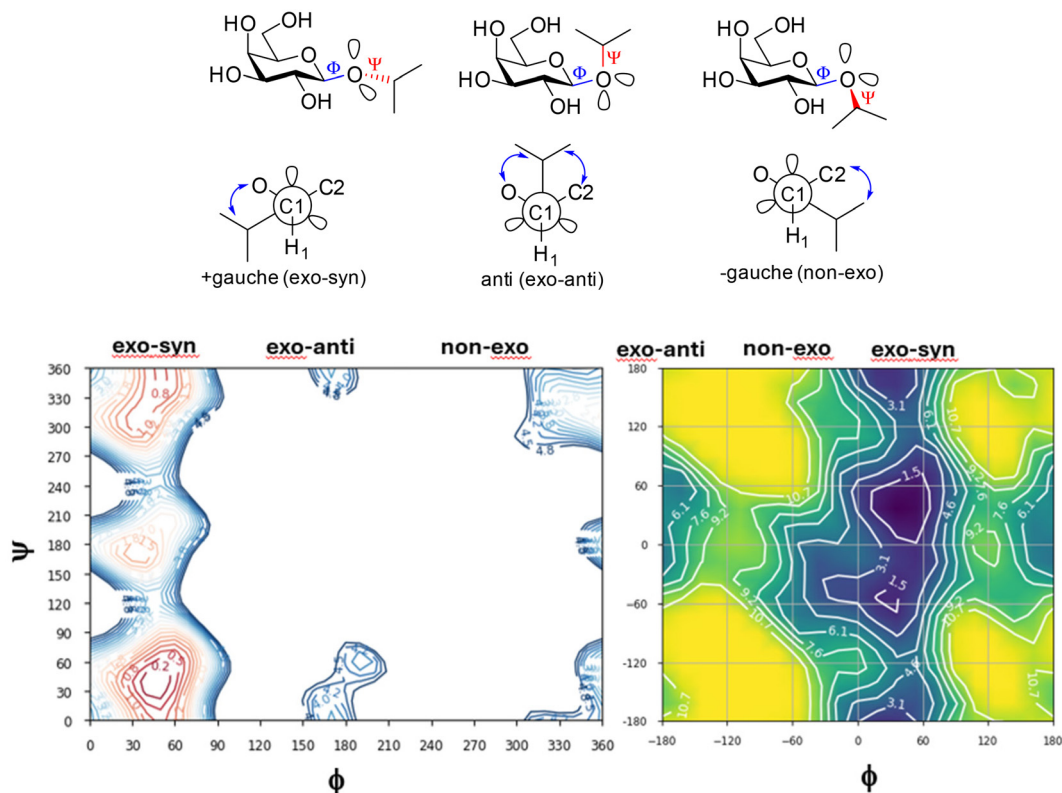


Fig. 1 Chemdraw structures and Newman projections for conformers of isopropyl β -D-galactopyranoside (IPG). The plot on bottom left shows the output from coordinate scan plots (OPLS4 force field) obtained from MacroModel while applying the water GBSA model. Contours are those within 5 kcal mol^{-1} of the lowest energy conformer and there are $0.25 \text{ kcal mol}^{-1}$ differences between contour lines, with energy increasing from red to blue. The plot on the right is the energy surface from 10 ns metadynamics simulation performed in water. Energy (kcal mol^{-1}) increases from blue/navy to yellow. The dihedral angle ϕ is defined by atoms $\text{H1-C1-O-C}_{\text{IPr}}$ and ψ by $\text{C1-O-C}_{\text{IPr}}-\text{H}_{\text{IPr}}$. The metadynamics and coordinate scans predict similar global minimum conformers ($\phi = \text{exo-syn}$ or $+$ *gauche*; $\psi = +$ *gauche*). The term *exo* refers to the conformers where the *exo*-anomeric effect occurs.

OD_{600} values). SDS PAGE, electrotransfer of proteins on PVDF membrane, and protein detection were carried out as previously described³⁵ using Fisher BioReagents™ EZ-Run™ Pre-stained Rec Protein Ladder as a marker. The horseradish peroxidase-labelled monoclonal antibody (A7058, Sigma) recognizing the His6-mTFP1 fusion protein and Pierce™ 1-Step Ultra TMB Blotting solution (ThermoFisher Scientific) were used to develop the western blot. A representative western blot of three independent experiments is shown in Fig. 4, middle panel. In parallel, the same bacterial samples were analysed by SDS PAGE and stained with Coomassie Brilliant Blue to verify equal loading samples (data not shown). The lower panel shows the growth of *E. coli* Rosetta strain harboring the pET28 vector expressing green fluorescent protein in the absence and presence of 1 mM of IPTG **1** and **2**. At the indicated time points, culture samples were collected and the OD_{600} were measured.

The results (Fig. 4, top and middle panel) show that **2** is an effective inhibitor of the lac repressor protein, leading to induction of protein expression with a similar expression level at 4 h and 24 h of addition as with IPTG (top panel), whereas the other C-glycosides are much less effective. Cyclic acetal **6** and the ketone **7** showed the capability to induce protein pro-

duction but to a lesser degree than **1** and **2**. Similar results were found using bacteria expressing green fluorescent protein (GFP) using the vector pET28 BL21(DE3) Rosetta as a host (data not shown).

The mTFP1 expression was verified using western blotting (Fig. 4, middle panel). The western blot shows that in the absence of IPTG and **2** a minimal amount of mTFP1 is produced, which does not increase during culturing. In contrast, both compounds, **1** and **2**, efficiently induce the production of recombinant protein as early as 1 h after their addition to bacterial cultures and the protein expression increases with time (Fig. 4, middle panel). Interestingly, IPTG-treated samples show partial proteolytic degradation of mTFP1 as soon as 1 h, which was not seen in the **2**-treated samples even after 2 h (Fig. 4, middle panel compare lanes 5 and 6 with lanes 8 and 9, respectively).

To further analyze the influence of **1** and **2** on *E. coli*, bacteria cultures were treated with 1 mM of **1** and **2** and their growth was compared with bacteria grown in the absence of these compounds. The growth curves of *E. coli* treated with **1** showed a significant reduction of the cell numbers over time in comparison to untreated and **2**-treated cells (Fig. 4, lower panel).



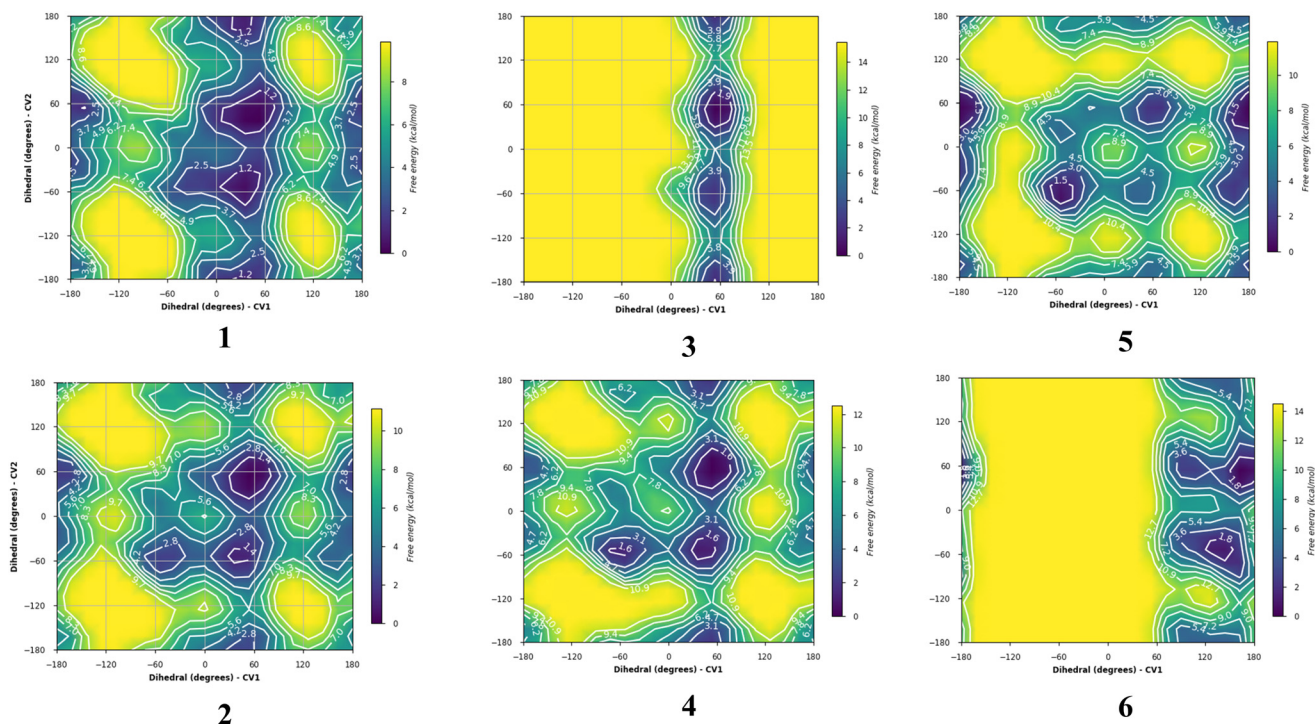


Fig. 2 Plots showing relative energy (kcal mol^{-1}) from metadynamics simulations where the collective variables $\text{CV1} = \phi$ and $\text{CV2} = \psi$. The simulations were performed in water boxes (with explicit water).

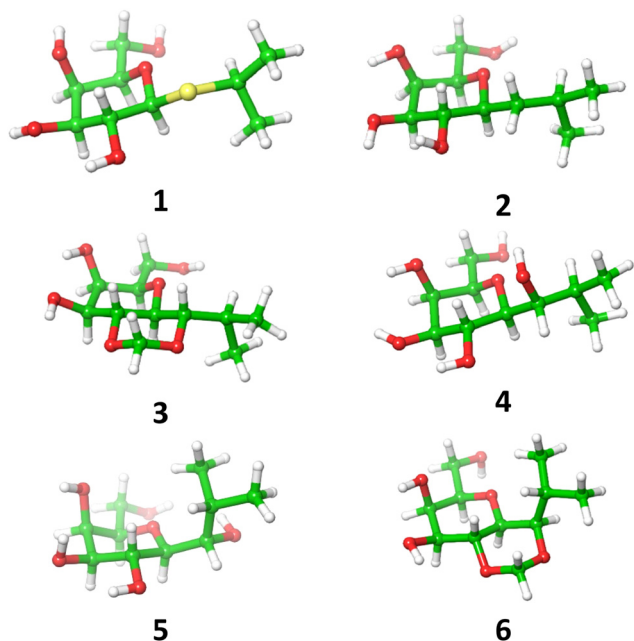


Fig. 3 Low energy conformers for 1–6 obtained from metadynamics simulations in explicit water.

In summary, these findings suggest that 1- β -D-galactopyranosyl-2-methylpropane 2 is an improved inducer of protein expression using the lac repressor compared to IPTG 1. Compound 2 induces similar levels of proteins as determined by two independent methods (Fig. 4 top and middle panel)

but with less proteolytic degradation of the recombinant protein as seen with mTFP1 (Fig. 4, middle panel) and an additional recombinant protein LSSmOrange (data not shown). A reduced level of proteolysis allows an easier purification of full-length protein and thus is a marker for improved quality of the recombinant protein important for biochemical, biotechnological and pharmaceutical products and studies. It is known that the addition of IPTG 1 reduces bacterial growth; this has been proposed to be due to stressing the bacteria due to metabolic burden caused by the increased protein synthesis but recently it was shown that metabolic degradation products of IPTG 1 cause additional stress to the bacteria expressing proteins. In contrast, the natural effector lactose³⁶ and 1- β -D-galactopyranosyl-2-methylpropane 2, a subject of this work, caused less stress to the bacteria than 1.

2.4 Investigation of repressor binding to IPTG and C-glycosides by molecular simulations

The interactions of the C-glycoside compounds with the lac repressor were next explored by molecular modelling methods, to try to rationalise the different properties displayed by 1–6.

2.4.1 Protein preparation for docking and molecular dynamics. The crystal structure providing atomic details of IPTG 1 bound to the lac repressor at 2.0 Å resolution has been reported by Lewis and co-workers;³⁷ the coordinates are that of a protein dimer with two IPTG ligands in identical binding sites and the downloaded structure was subjected to the protein preparation workflow in Maestro which involved assigning bond orders, replacement of hydrogen atoms and



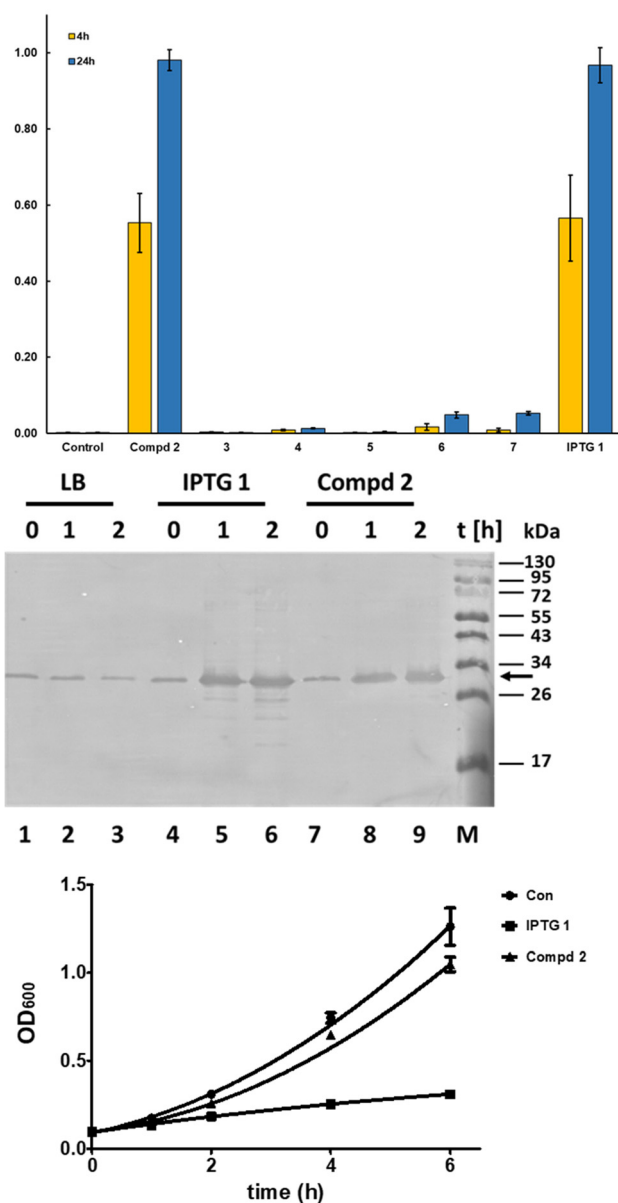


Fig. 4 Compd 2 induces expression of recombinant proteins in bacteria with high efficiency. In the top panel, the time-dependent mTFP1 expression as determined after treatment of *E. coli* with glycomimetics is shown. The mTFP1 expression was verified by western blotting (middle panel). The arrow on the right indicates the full length recombinant His₆-mTFP1. The lower panel shows the growth of *E. coli* BL21 (DE3) Rosetta strain harboring the pET28 vector expressing GFP in the absence and presence of 1 mM of IPTG and 2. At the indicated time points, culture samples were collected and their OD₆₀₀ values were measured. The results, top and lowest panel, are the average and standard deviation of three experiments. The middle panel presents a representative western blot of three independent experiments.

generation of protonation states (pH = 7.4), followed by optimization of H-bonding interactions, energy minimization including the removal of any crystallized water molecules at more than 5 Å distance from the ligands. The crystal structure showed *+gauche* conformations for both ϕ (+52°) and ψ (+60°) in the two IPTG binding sites; ϕ was +47° and +46° in the two

sites after protein preparation, and ψ was *+gauche* at both sites (+51°, +51°). Each IPTG ligand showed identical interactions with the receptor. The galactopyranoside 4- and 6-OH groups engaged in water mediated (indirect) H-bonding interactions with protein (4-OH to Gln248 and 6-OH to Asp149), the 2-OH and 3-OH were involved in direct H-bond donation to Asp274, while the 3-O accepts H-bonds from the side chain of Arg197 and one H-bond from Asn246. The isobutyl group was in a pocket that had water molecules as well as the side chains of Ser193, Leu148, Ile79 were all within 3 Å of the H atoms. The β -face of the galactopyranosyl group, specifically H-3, H-4 and H-5, stack against the indole residue of Trp220 constituting a CH- π interaction.³⁸ The X-ray crystal structure showed water mediated interactions of the 6-OH, proposed by Lewis and co-workers to crosslink the N- and C-terminal subdomains of the lac repressor, and direct H-bonding between Ser193 and Asp149 was evident, the latter being implicated in transmitting the allosteric signal through the N-terminal sub-domain to the DNA binding domain of the repressor.

2.4.2 Glide docking and MMGBSA study of ligands 1–6 and IPG. The binding of ligands was explored using Glide docking³⁹ implemented with Maestro. For structures 2, 4 and 5 and IPG the poses and orientation of the iPr and H-bonding interactions generated by the docking were similar or identical with that of IPTG. While IPTG 1 gave the best glide score, the scores for the best poses had a rank 1 > 5 > 2 > 4 > IPG and all had similar scores. The cyclic constrained compounds had significantly lower scores with steric repulsion interactions leading to the galactopyranose residue being significantly shifted from the position adopted in 1. Subsequently the poses generated were subjected to molecular mechanics with generalised Born and surface-area solvation (MMGBSA⁴⁰) study as implemented in Maestro. MMGBSA is a method to estimate protein–ligand binding affinities and this also predicted higher affinity for the lac repressor for IPG, 1, 2, 4 and 5 compared to 3 and 6, with the highest affinity predicted for IPG. Thus, the docking indicated the lac repressor had the potential to bind 2, 4 and 5 with good affinity, with 4 predicted to have higher affinity than 1 by MMGBSA. The application of MMGBSA in this context appears to have limitations as it did not explain the previously observed higher affinity of 1 for the repressor compared to IPG.

2.4.3 Binding pose metadynamics.⁴¹ Metadynamics simulations are based on varying a small number of parameters, collective variables (CVs), and exploring the impact of varying these parameters on the energy of the system. In binding pose metadynamics the X-ray crystal coordinates provide a basis for varying ligand pose and investigating how various starting poses influences binding energy. The CV is the measure of the root-mean-square deviation (RMSD) of the ligand heavy atoms relative to their starting position. The protocol for Desmond binding pose metadynamics using OPLS4 was implemented for 1 in Maestro. Before the simulation, the protein and ligand were placed in an orthorhombic box of SPC water molecules, using the Desmond system builder, with a buffer of 10 Å between the solute structures and the simulation box bound-



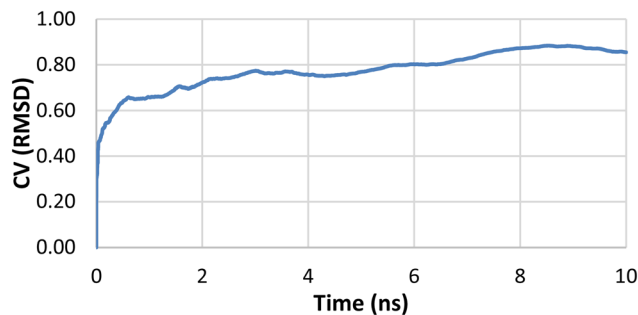


Fig. 5 A plot of average RMSD from 10 trials of IPTG heavy atoms from binding pose metadynamics.

ary on each axis. The IPTG **1** in site A was subjected to BPMD from 10 trials generated, each subjected to 10 ns molecular dynamics, with 50 structures sampled for each trial. The RMSD of ligand atom positions is plotted vs. simulation time, averaging over 10 trials (Fig. 5). The PoseScore, is the RMSD of the ligand with respect to the initial ligand heavy atoms coordinates and a value ≤ 2 Å is considered stable, as observed here, and is based on the final 2 ns of the simulation. A PersScore of >0.6 (60% of H bonds kept during the simulation) is an indication of strong hydrogen bonding between the ligand and the protein residues. For **1** a PoseScore of 0.873 and PersScore of 0.898 was determined. For IPTG **1** the direct H-bonds of the 2 and 3-OH groups of the galactopyranoside with Asp27 were found to have $>98\%$ occurrence; two H-bonds to Arg197 had 100% and 70% occurrence and the H-bond to Asn246 80% occurrence during the simulation. Thus, the galactopyranose residue of **1** forms stable and strong H-bonding interactions with the repressor.

2.4.4 Metadynamics for bound IPTG with ϕ and ψ as the collective variables. The BPMD analysis did not take into consideration flexibility of the isopropyl residue, which we observed on examination of the MD trajectories obtained in the BPMD trials. A metadynamic simulation (10 ns) was carried out with coordinates of IPTG bound in the repressor, with ϕ and ψ as the collective variables and the surface energy plot obtained is shown in Fig. 6. The lowest energy bound conformation calculated (OPLS4 force field) corresponded to the ϕ *-gauche* (-46°), with ψ close to eclipsed ($+16^\circ$); this corresponds to conformers also observed during BPMD (data not shown); this conformational preference is significantly different to that observed for (i) bound IPTG in the crystal structure, and (ii) unbound IPTG in presence of explicit water (see Fig. 2 for metadynamics) and in the gas phase. It was noticed that water molecules in the original crystal structure near the isopropyl group were displaced by hydrophobic residues in the area within 3 Å of the iPr hydrogens during the simulations, with this exclusion of water being associated with the IPTG conformational change.

2.4.5 Longer molecular dynamics simulations. Molecular dynamics simulations of 100 ns were performed for **1**, **2**, **4** and **5** as ligands for the repressor, to compare the trajectories to try to predict why **4** and **5** might not be inducers. Again, the protein and ligands were solvated in orthorhombic boxes of

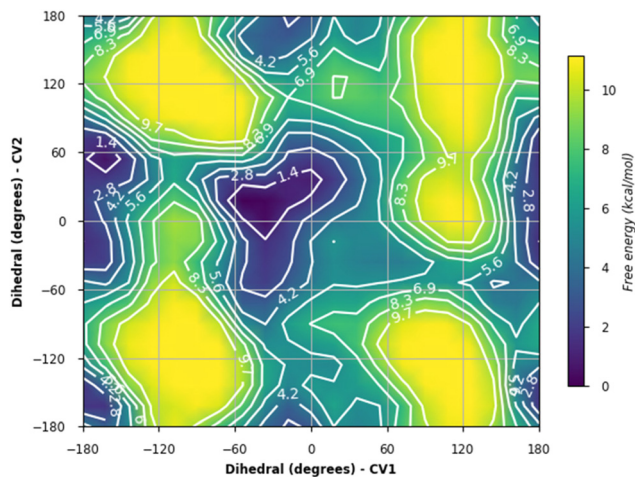


Fig. 6 Energy surface plot from metadynamics of IPTG **1** bound to the lac repressor where ϕ (CV1) and ψ (CV2) were the collective variables.

SPC water molecules, with buffers of 10 Å between the solute structures and the simulation box boundary on each axis and subjected to simulations with Desmond with one structure sampled at every 0.2 ns time point giving 500 structures overall.

The Desmond analysis reports for each 100 ns simulation is provided in the SI. These reports include monitoring of (i) protein–ligand RMSD values (ii) protein root mean square fluctuation (RMSF), (iii) secondary structure elements (iv) ligand root mean square fluctuation (v) protein–ligand contacts (vi) ligand torsional profiles and (vii) ligand properties such as solvent accessible surface areas and polar surface areas. The root mean square deviation (RMSD) measured the average change in displacement of protein atoms with respect to the starting structure and did not exceed 2 Å in the presence of the ligands studied, indicating there was no major conformational change to protein during the simulation. In the final 10 ns of the simulation for IPTG and the protein, the protein RMSD stabilised at <1.25 Å relative to the starting structure. For protein bound to **2**, **4** and **5**, the protein RMSD stabilised at <2 Å in the final 20 ns relative to the starting structure, again barely exceeding 2 Å at any stage in the simulations.

The fraction of interactions for each ligand for the first 10 ns (0–10 ns) was compared with the final 10 ns (90–100 ns) during the simulation in Fig. 7. The analysis for IPTG **1** showed that all main direct and indirect H-bonding interactions between protein and ligand mediated by water, as well as the CH– π interaction with Trp220 were preserved throughout the 100 ns simulation. For inducer **2**, most of the same interactions as IPTG **1** persisted throughout and the direct H-bond interaction between Ser193 and Asp149 occurred frequently for both. For **4** there was the emergence of a direct H-bond of the isobutyl OH with either Asp149 or with Asn125, these being different outcomes from two independent simulations. When the interaction with Asn125 occurred, there was a significant reduction in other interactions, such as removal of direct H-bond between Asn246 and the galactopyranosyl 3-OH and the distance between Ser193 and Asp149 increased,



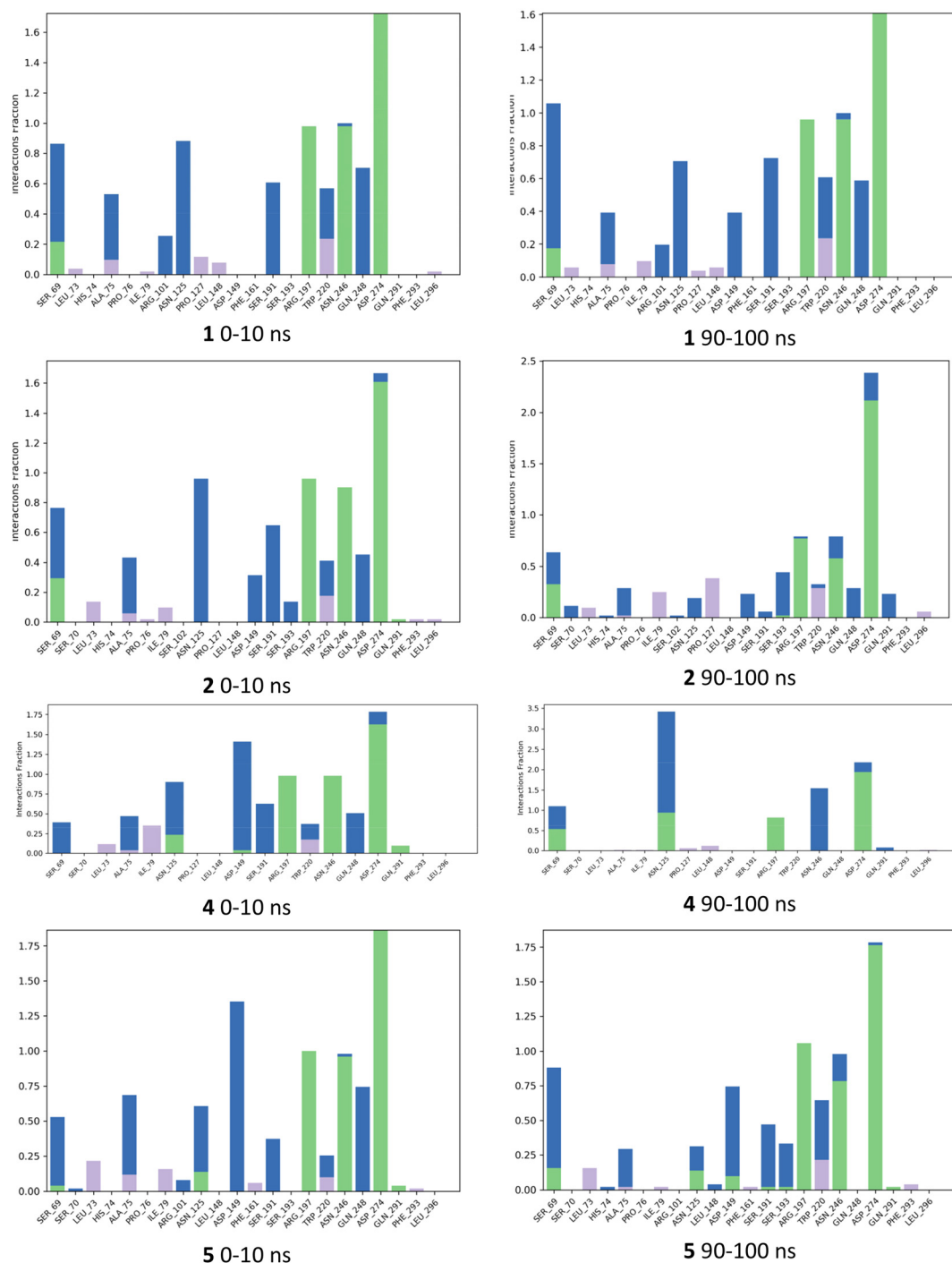


Fig. 7 Histograms summarizing fraction of occurrence of ligand protein contacts from selected molecular dynamics simulations. Green = direct H bonds, blue = indirect H bonds, purple = hydrophobic interactions, including CH– π interactions.

precluding H-bonding between these residues. We, thus, speculate that the additional OH group may disrupt the complex network of interactions that are required for inhibition of the repressor such as the interaction between Ser193 and Asp149. Direct H-bonding from the aglycon OH was seen to occur during the simulation for 5 although it was not as frequent as for 4 and the interaction between Ser193 and Asp149 occurred more frequently for 5. The simulations for 5 did

show direct H-bond interaction between Ser193 and Asp149 for much of the simulation comparable to 1 and 2.

The values for ϕ and ψ during the simulations were also examined. For 1, the conformation changed from that of the crystal structure; this had occurred within the first 10 ns and persisted for the full length of the simulation. While 1 and 2 showed similar interactions, there was a difference in terms of ϕ and ψ in conformers sampled during the simulations (Fig. 8);



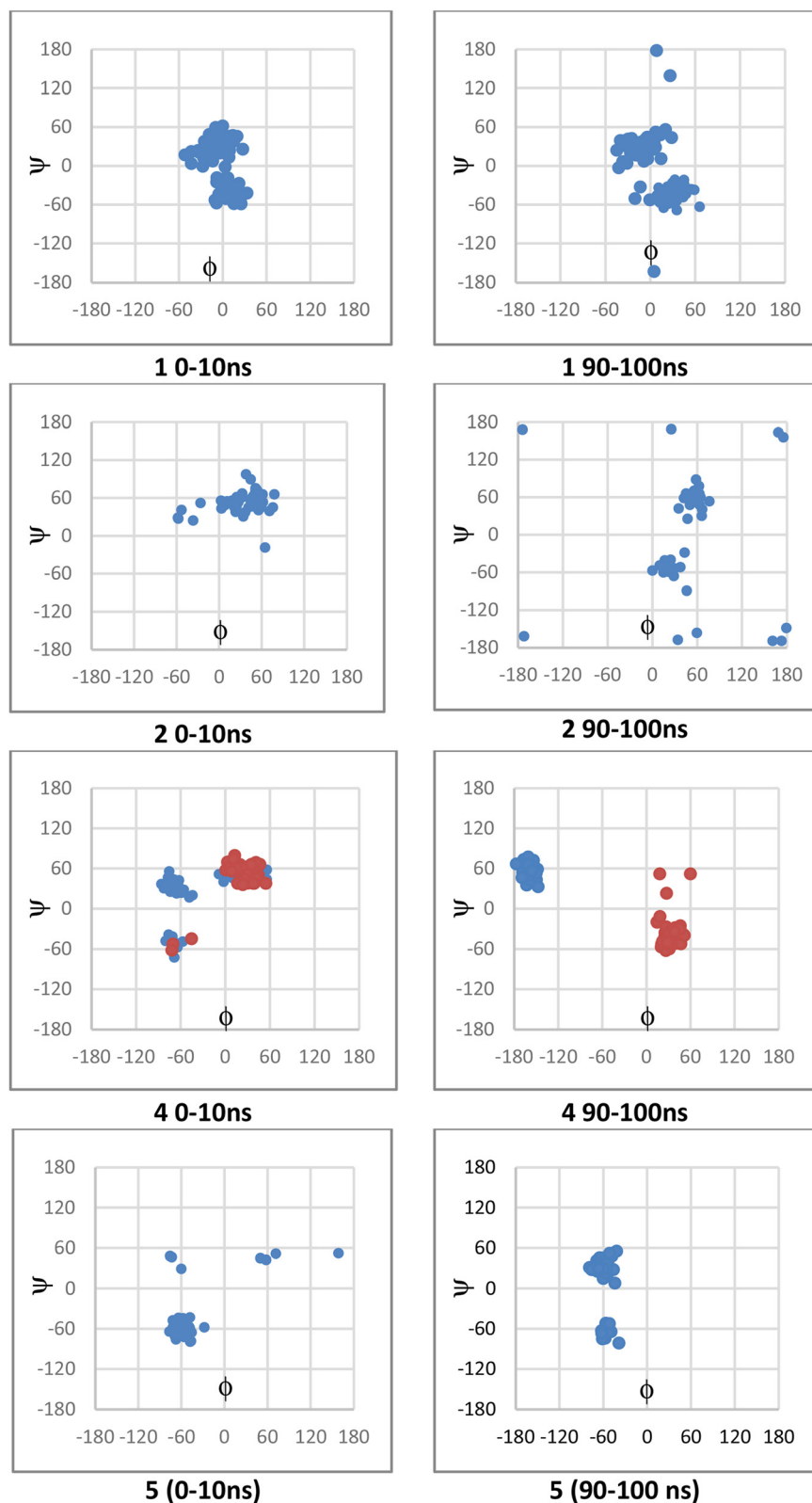


Fig. 8 Scatter plots showing ϕ and ψ from structures sampled during molecular dynamics simulations on the left are from 0–10 ns and on right from 90–100 ns. The red and blue data for 4 correspond to data from two simulations; the red occurred when there is direct H-bond interaction of the isobutanol OH with Asn125, whereas the blue there is direct interaction of this OH with Asn149.



2 was more likely than 1 to adopt ϕ +gauche and ψ +gauche conformer, with 2 being preorganized for binding in this manner; although 2 showed at 90–100 ns sampling of ϕ eclipsed to ϕ +gauche and ψ –gauche conformers like 1, as well as the ϕ +gauche and ψ +gauche. The values for ϕ and ψ for 4, depended on whether there was a direct H-bond to Asp149 or Asn125; a direct H-bonding interaction to Asp149 at 90–100 ns leads to the bound conformation being ϕ +gauche and ψ anti; if the interaction occurred with Asn125 then the ϕ +gauche and ψ –gauche is bound; in the 0–10 ns timeframe before these H-bonding interactions arose there was adoption of the ϕ +gauche and ψ +gauche. For 5, ϕ = –gauche conformers were mostly bound throughout, showing +/– gauche for ψ at 90–100 ns indicating that 5, bound or unbound, does not mimic favoured conformation of 1 or 2.

2.5 Evaluation of compounds as β -galactosidase inhibitors

The *C*-glycosides were evaluated as inhibitors of β -galactosidases according to the procedure published previously by Bols *et al.*⁴² and the data is shown in Table 2. IPTG 1 is an inhibitor and has a previously reported inhibition constant (K_i) value of 0.08 mM for the native *E. coli* (*lacZ*) β -galactosidase;⁴³ the value we obtained was 0.199 mM. This type of inhibitor is weaker than the iminosugar type.⁴⁴ The best inhibitor in this series was 2, with ~2-fold improvement seen relative to 1. Compound 2 showed a 6-fold improvement over 1 as an inhibitor of the β -galactosidase from *A. niger*, while 6 showed improved K_i value compared to that of 2 for the α -galactosidase from *A. niger*. The crystal structure of IPTG 1 bound to the *E. coli* β -galactosidase has been determined (PDB ID: 1JYX),⁴⁵ where the IPTG is bound as the conformer where ϕ = +77° (+gauche) and ψ = –41° (–gauche), the closest conformer to this from the DFT study is 1g. When the coordinates for 1JYX were subjected to protein preparation the ϕ changed to +52° (+gauche) and ψ = –35° (–gauche). The IPTG 1 showed direct H-bond donation from the 2-OH to Glu461 and from 3-OH to Glu537, while the ring oxygen accepted a H-bond from Asn102 and 6-O from His540 and the 6-O also coordinates to a sodium ion; there was also indirect H-bonding (Fig. 9). The isopropyl residue contributes to CH– π interactions with Trp999 which is also close to CH protons of the galactose. Similar K_i values especially between 1, 3 and 6 indicate that the enzyme has some flexibility and can accommodate different orientations of the iPr group. It maybe that the iPr of 2 is preorganised similarly to 3, while 2 can also have the H-bond between its 2-OH and Glu461, that explains 2's higher affinity. Although 4 would also be preorganised, there is no benefit to the presence of its extra OH.

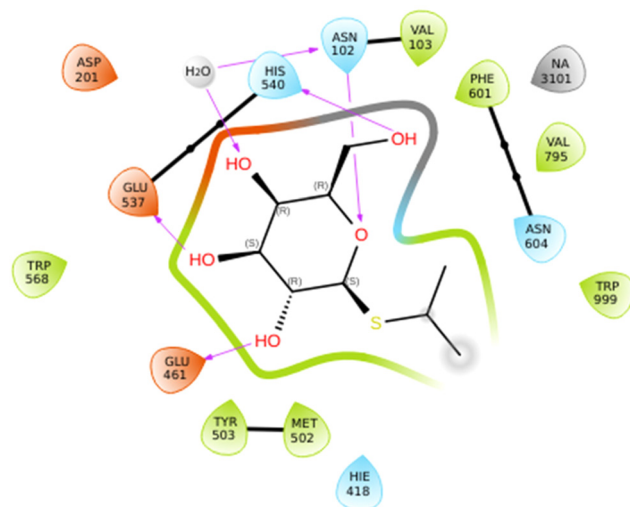


Fig. 9 Ligand interaction diagram for IPTG 1 binding to *E. coli* β -galactosidase. This diagram was generated in Maestro after subjecting coordinates for PDB 1JYX to protein preparation wizard implemented in Maestro.

3. Summary and conclusions

Small *C*-glycoside mimetics of IPTG, 2–7, have been synthesised to investigate their ability to induce protein synthesis *via* allosteric binding to *E. coli*'s lac repressor and influence the repressor's interaction with DNA. Galactopyranose is an essential component of inducer structure, making strong direct H-bonding interactions with the repressor, with its 6-OH is involved in H-bonding network involving indirect H-bonding *via* water molecules, that may be involved in stabilizing a repressor conformation that has low affinity for DNA. The nature of galactopyranose's anomeric substituent also determines whether a substance reduces (inducer) or increases (anti-inducer) affinity of the lac repressor for DNA or whether it is a binder but does not increase rate of protein synthesis. Newly synthesized *C*-glycosides 3–7 did not induce protein synthesis effectively when compared to the standard inducer IPTG 1 and another known inducer 1- β -D-galactopyranosyl-2-methylpropane 2. Interestingly, 1- β -D-galactopyranosyl-2-methylpropane 2 yielded reduced proteolysis of the expressed test proteins compared to 1; the latter observation could be significant in terms of generating proteins with more straightforward purification protocols and improved quality of the purified protein for biochemical, biotechnological, and pharmaceutical purposes.

The study of conformation of 1–6 showed parallels between metadynamics simulations with conformation derived by the

Table 2 Inhibition constants (K_i) in mM of 1–6 measured at 26 °C

Enzyme	1	2	3	4	5	6
β -Galactosidase (<i>E. coli</i>)	0.199 \pm 0.066	0.0882 \pm 0.024	0.176 \pm 0.094	0.230 \pm 0.138	0.372 \pm 0.233	0.198 \pm 0.086
β -Galactosidase (<i>A. Niger</i>)	12.1 \pm 4.7	2.00 \pm 1.03	3.27 \pm 1.52	0.832 \pm 0.430	—	—
α -Galactosidase (<i>A. Niger</i>)	—	24.8 \pm 12.3	—	—	—	2.92 \pm 1.30



analysis of the $^3J_{\text{HH}}$ values obtained by $^1\text{H-NMR}$ in methanol- d_4 and for **2** in water. For inducer **2**, the major conformation was analogous to that calculated for the *O*-glycoside, isopropyl β -D-galactopyranoside (ϕ +*gauche* and ψ +*gauche*). The *S*-glycoside **1** appears to be more flexible than *C*- or *O*-glycosides based on the metadynamics, evident in energy contour plots. Thus, molecular dynamics simulations (BPMD or longer MD simulation) indicated that **1** shows flexibility in the binding pocket of the lac repressor, that the *iPr* orientation changes from that observed in the crystal structure; the conformational change for **1** does not appear to significantly disrupt the interaction between repressor's Ser193 and Asp149 or H-bonding network that may be required to adopt a conformation that reduces affinity for DNA. While the orientation of the *iPr* group in the binding site was different for **2** compared to **1**, **2** sustained interactions like those observed for IPTG **1** over 100 ns MD simulations including that between Ser193 and Asp149, linked with low affinity conformation of the repressor for DNA binding. For the cyclic acetal derivatives **3** and **6**, the loss of 2-OH mediated H-bonding to the repressor would be predicted to lead to reduced affinity of these substances; however, **6** sustained weak inducer activity and its mode of binding is unclear. For the isobutanols **4** and **5**, MD simulation led to prediction that generation of new H-bonding interactions could disrupt the H-bonding network. Clearly the factors which determine whether a substance can be an inducer or negative inducer/neutral effector are complex and will need further investigation. Synthesis of further constrained *C*-glycosides lacking H-bond disrupting group in the isobutyl residue, and/or determination of further co-crystal structures of *C*-glycosides with the lac repressor will be needed to give further insight. Finally, the insight from evaluation of various constrained *C*-glycosides as galactosidase inhibitors shows that there may be flexibility in how this enzyme recognizes the aglycon group in its binding pocket. The synthesis and analysis, described here, provide the basis for synthesis of conformationally constrained galactopyranoside mimetics, which have wide biological relevance, such as for lectins. Our research in galectin inhibitor identification based on related *C*-glycoside scaffolds as β -galactoside mimetics, will be disclosed in due course.

4. Experimental section

4.1 1-(β -D-Galactopyranosyl)-2-methylpropane (**2**)

Compound **20** (350 mg, 0.90 mmol) was dissolved in MeOH and Pd-C (10%) was added to the reaction mixture. The flask was fitted with a H_2 balloon and stirred overnight, and the mixture was then filtered through Celite and the solvent was removed under reduced pressure. Flash chromatography (cyclohexane-EtOAc 4 : 1) provided the acetylated intermediate (327 mg, 93%) as a white solid; R_f 0.56 (cyclohexane-EtOAc 4 : 1); HRMS calcd for $\text{C}_{18}\text{H}_{32}\text{NO}_9$ [$\text{M} + \text{NH}_4$] $^+$ 406.2071 found m/z 406.2021. The NMR data (see ESI †) for the intermediate obtained was in good agreement with that reported pre-

viously.¹⁶ The intermediate (550 mg, 1.42 mmol) was dissolved in dry methanol (5.5 mL) and sodium methoxide (8 mg, 0.15 mmol) was added and the mixture was then stirred at room temp for 15 minutes. Amberlite (H^+) was added to neutralise the reaction mixture after which the solvent was evaporated under reduced pressure and chromatography of the residue (silica gel, elution with 10 : 1 acetonitrile-ammonium hydroxide) gave the title compound **2** (240 mg, 77%) as a white solid. $^1\text{H-NMR}$ (400 MHz, CD_3OD) δ 3.84 (dd, J = 3.3, 1.1 Hz, 1H, H-4), 3.66 (dd, J = 11.3, 6.7 Hz, 1H, H-6a), 3.63 (dd, J = 11.2, 5.8 Hz, 1H, H-6b), 3.41–3.36 (overlapping signals, 2H, H-3 & H-5), 3.31 (d, J = 9.2 Hz, 1H, H-2), 3.11 (td, J = 10.0, 9.1, 2.1 Hz, 1H, H-1), 1.89 (m, 1H, isopropyl CH), 1.59 (ddd, J = 14.0, 9.7, 2.1 Hz, 1H, *CHH*), 1.39 (ddd, J = 14.2, 10.0, 4.3 Hz, 1H, *CHH*), 0.91 (d, J = 6.8 Hz, 3H), 0.88 (d, J = 6.6 Hz, 3H); $^{13}\text{C-NMR}$ (126 MHz, CD_3OD) δ 78.61 (C-5), 78.34 (C-1), 75.08 (C-3), 71.80 (C-2), 69.36 (C-4), 61.26 (C-6), 40.67 (C-1'), 24.12 (C-2'), 22.91, 20.69 (each CH_3). The NMR data obtained was in good agreement with that reported previously.¹⁶ Selected $^1\text{H-NMR}$ data for **2** obtained from sample dissolved in D_2O (500 MHz): δ 3.30 (ddd (apt td), J = 9.7, 9.9, 2.1 Hz, 1H, H-1), 1.85 (dheptd, J = 9.9, 6.8 ($\times 6$), 4.3 Hz, 1H, isopropyl CH), 1.58 (ddd, J = 14.4, 9.9, 2.2 Hz, 1H, *CH(H)CHMe*), 1.42 (ddd, J = 14.3, 9.9, 4.3 Hz, 1H, *CH(H)CHMe*).

4.2 (4*S*,4*aS*,6*R*,7*R*,8*S*,8*aR*)-6-(Hydroxymethyl)-4-isopropylhexahydroprano[3,2-*d'*][1,3]dioxine-7,8-diol (**3**)

Benzylated **18** (115 mg, 0.22 mmol) was dissolved in dry methanol (5 mL), and Pd-C (10%; 115 mg, 100% w/w) was added. The round-bottom flask was fitted with a gas bag filled with hydrogen gas and the reaction mixture was stirred at room temperature for 16 h. The reaction mixture was then filtered through Celite, and the solvent was removed under reduced pressure. Chromatography (silica gel, eluting with 10 : 1 acetonitrile-aqueous ammonium hydroxide) gave **3** (42 mg, 76%) as a white solid; R_f 0.4 (CH_2Cl_2 -MeOH 9 : 1); $^1\text{H-NMR}$ (500 MHz, CD_3OD) δ 5.03 (d, J = 6.1 Hz, 1H, methylene *CHH*), 4.70 (d, J = 6.1 Hz, 1H, methylene *CHH*), 3.91 (dd, J = 3.5, 1.3 Hz, 1H, H-4), 3.73–3.64 (overlapping signals, 3H, H-3, H-6a & H-6b), 3.56 (t, J = 9.5 Hz, 1H, H-2), 3.53 (ddd, J = 6.6, 5.3, 1.3 Hz, 1H, H-5), 3.37 (dd, J = 9.3, 2.8 Hz, 1H, H-1'), 3.08 (t, J = 9.1 Hz, 1H, H-1), 2.08 (heptet of doublets, J = 7.0, 2.8 Hz, 1H, isopropyl CH), 1.00 (d, J = 7.0 Hz, 3H, CH_3), 0.92 (d, J = 7.0 Hz, 3H, CH_3); $^{13}\text{C-NMR}$ (126 MHz, CD_3OD) δ 93.45 (methylene CH_2), 82.61 (C-1'), 79.60 (C-5), 78.19 (C-2), 73.56 (C-1), 71.74 (C-3), 69.61 (C-4), 61.24 (C-6), 27.77 (C-2'), 18.23, 14.70 (each CH_3); HRMS calcd for $\text{C}_{12}\text{H}_{23}\text{O}_6\text{Na}$ [$\text{M} + \text{Na}$] $^+$ 271.1152 found m/z 271.1154.

4.3 (2*S*,3*R*,4*S*,5*R*,6*R*)-2-((*R*)-1-Hydroxy-2-methylpropyl)-6-(hydroxymethyl)tetrahydro-2*H*-pyran-3,4,5-triol (**4**)

Compound **13** (130 mg, 0.256 mmol) was dissolved in dry methanol (5 mL), and Pd-C (10%; 130 mg, 100% w/w) was added. The round-bottom flask was fitted with a gas bag filled with hydrogen gas and the reaction mixture was stirred at room temperature for 16 h. The reaction mixture was then fil-



tered through Celite, and the solvent was removed under reduced pressure. Chromatography (silica gel, eluting with acetonitrile and aqueous ammonium hydroxide solution (10:1)) gave **4** (32 mg, 53%) as a white solid; $^1\text{H-NMR}$ (500 MHz, CD_3OD) δ 3.85 (dd, $J = 3.3, 1.1$ Hz, 1H, H-4), 3.79 (t, $J = 9.6$ Hz, 1H, H-2), 3.70 (dd, $J = 11.4, 6.6$ Hz, 1H, H-6a), 3.67 (dd, $J = 11.4, 5.6$ Hz, 1H, H-6b), 3.47–3.41 (overlapping signals, 2H, H-3 & H-5), 3.38 (dd, $J = 8.8, 1.6$ Hz, 1H, H-1'), 3.22 (dd, $J = 9.5, 1.6$ Hz, 1H, H-1), 1.94 (doublet of heptets, $J = 8.7, 6.7$ Hz, 1H, isopropyl CH), 1.02 (d, $J = 6.8$ Hz, 3H), 0.89 (d, $J = 6.7$ Hz, 3H) (each CH_3); $^{13}\text{C-NMR}$ (126 MHz, CD_3OD) δ 79.16 (C-1), 78.80 (C-5), 75.46 (C-3), 74.15 (C-1'), 69.66 (C-4), 67.10 (C-2), 61.25 (C-6), 30.60 (C-2'), 18.80, 18.12 (each CH_3); HRMS calcd for $\text{C}_{10}\text{H}_{20}\text{O}_6\text{Na}$ $[\text{M} + \text{Na}]^+$ 259.1152 found m/z 259.1153.

4.4 (2*S*,3*R*,4*S*,5*R*,6*R*)-2-((*S*)-1-Hydroxy-2-methylpropyl)-6-(hydroxymethyl)tetrahydro-2*H*-pyran-3,4,5-triol (**5**)

Alcohol **17** (150 mg, 0.239 mmol) was dissolved in dry methanol (5 mL), and Pd-C (10%; 150 mg, 100% w/w) was added. The round-bottom flask was fitted with a gas bag filled with hydrogen gas and the reaction mixture was stirred at room temperature for 16 h. The reaction mixture was then filtered through Celite, and the solvent was removed under diminished pressure. Column chromatography (silica gel eluting with acetonitrile and aqueous ammonium hydroxide solution (10:1)) gave **5** (35 mg, 62%) as a white solid; $^1\text{H-NMR}$ (500 MHz, CD_3OD) δ 3.89 (d, $J = 3.2$ Hz, 1H, H-4), 3.78 (t, $J = 9.3$ Hz, 1H, H-2), 3.74 (dd, $J = 11.5, 6.7$ Hz, 1H, H-6a), 3.69 (dd, $J = 11.3, 4.9$ Hz, 1H, H-6b), 3.64 (t, $J = 5.2$ Hz, 1H, H-1'), 3.53–3.46 (overlapping signals, 2H, H-3 & H-5), 3.28 (dd, $J = 9.4, 5.8$ Hz, 1H, H-1), 2.09 (heptet of doublets, $J = 6.9, 4.6$ Hz, 1H, isopropyl CH), 0.97 (d, $J = 6.9$ Hz, 3H), 0.94 (d, $J = 6.7$ Hz, 3H) (each CH_3); $^{13}\text{C-NMR}$ (126 MHz, CD_3OD) δ 79.10 (C-1), 78.58 (C-5), 77.94 (C-1'), 75.00 (C-3), 70.04 (C-2), 69.55 (C-4), 61.66 (C-6), 29.11 (C-2'), 18.89, 15.80 (each CH_3); HRMS calcd for $\text{C}_{12}\text{H}_{23}\text{O}_6\text{Na}$ $[\text{M} + \text{Na}]^+$ 271.1152 found m/z 271.1158.

4.5 (4*S*,4*aS*,6*R*,7*R*,8*S*,8*aR*)-6-(Hydroxymethyl)-4-isopropylhexahydropyrano[3,2-*d*][1,3]dioxine-7,8-diol (**6**)

Compound **14** (90 mg, 0.173 mmol) was dissolved in dry methanol (5 mL), and Pd-C (10%; 90 mg, 100% w/w) was added. The round-bottom flask was fitted with a gas bag filled with hydrogen gas and the reaction mixture was stirred at room temperature for 16 h. The reaction mixture was then filtered through Celite, and the solvent was removed under reduced pressure. Chromatography (silica gel, eluting with 10:1 acetonitrile and aqueous ammonium hydroxide solution) gave **6** (28 mg, 65%) as a white solid; R_f 0.4 (CH_2Cl_2 –MeOH 9:1); $^1\text{H-NMR}$ (500 MHz, CD_3OD) δ 4.82 (d, $J = 6.5$ Hz, 1H, methylene *CHH*), 4.74 (d, $J = 6.4$ Hz, 1H, methylene *CHH*), 3.91 (dd, $J = 3.5, 1.3$ Hz, 1H, H-4), 3.86 (t, $J = 9.3$ Hz, 1H, H-2), 3.69 (dd, $J = 11.2, 6.5$ Hz, 1H, H-6a), 3.66 (dd, $J = 11.3, 5.5$ Hz, 1H, H-6b), 3.65–3.59 (overlapping signals, 3H, H-1, H-3 & H-1'), 3.48 (td, $J = 6.6, 5.4, 1.2$ Hz, 1H, H-5), 2.45 (doublet of heptets, $J = 10$ Hz, 6×6.5 Hz, 1H, isopropyl CH), 1.05 (d, $J = 6.3$ Hz, 3H), 0.95 (d, $J = 6.6$ Hz, 3H) (each CH_3); $^{13}\text{C-NMR}$ (126 MHz,

CD_3OD) δ 87.57 (methylene CH_2), 79.72 (C-5), 78.82 (C-1'), 75.88 (C-1), 72.90 (C-2), 72.53 (C-3), 69.50 (C-4), 61.40 (C-6), 24.57 (C-2'), 19.86, 18.64 (each CH_3); HRMS calcd for $\text{C}_{12}\text{H}_{23}\text{O}_6\text{Na}$ $[\text{M} + \text{Na}]^+$ 271.1152 found m/z 271.1154.

4.6 3,4,6-Tri-*O*-benzyl- β -thiopyridine-*D*-galactopyranose (**9**)

Glycal **7** (1.5 g, 3.60 mmol) was dissolved in dichloromethane (30 mL), acetone (3 mL) and saturated aqueous solution of sodium bicarbonate (50 mL) were added at 0 °C. The mixture was vigorously stirred and a solution of Oxone (6 g, 9.76 mmol) in water (25 mL) was added dropwise over 15 min. The reaction mixture was vigorously stirred at 0 °C for 30 min and was then warmed to room temperature until TLC indicated complete consumption of the starting material. The organic phase was separated, and the aqueous phase was extracted with dichloromethane (30 mL). The combined organic phases were dried with anhydrous sodium sulphate and concentrated under reduced pressure to afford the epoxide **8**⁴⁶ (1.6 g), which is sensitive to hydrolysis and was reacted without further purification. 2-Mercaptopyridine (1.03 g, 9.26 mmol) was dissolved in dry THF (10 mL) and the solution was cooled to 0 °C. Sodium hydride (370 mg, 9.26 mmol, 60% w/w in mineral oil) was added and the mixture was stirred at 0 °C for 15 minutes. Then a solution of freshly prepared epoxide **8** (2 g, 4.62 mmol) in dry THF (20 mL) was slowly added to the reaction mixture at 0 °C. The reaction mixture was then warmed to room temperature and stirred for 2 h. Upon completion of reaction using TLC, 10% aqueous solution of HCl (10 mL) was added. The reaction mixture was then extracted with ethyl acetate (30 mL \times 2). The combined organic layers were washed with water (20 mL \times 2) and dried with anhydrous sodium sulphate. The solvent was evaporated under reduced pressure, and chromatography (silica gel, eluting with 5:1 cyclohexane and ethyl acetate) gave **9** (2.16 g, 86%) as a pale yellow solid; $^1\text{H-NMR}$ (500 MHz, CDCl_3) δ 8.42 (d, $J = 4.5$ Hz, 1H), 7.47–7.22 (m, 17H), 7.04 (td, $J = 5.7, 1.6$ Hz, 1H) (each Ar-H), 5.22 (d, $J = 9.8$ Hz, 1H, H-1), 4.94 (d, $J = 11.4$ Hz, 1H), 4.81 (d, $J = 12.7$ Hz, 1H), 4.78 (d, $J = 12.7$ Hz, 1H), 4.62 (d, $J = 11.4$ Hz, 1H), 4.49 (d, $J = 11.8$ Hz, 1H), 4.43 (d, $J = 11.7$ Hz, 1H) (each Bn- CH_2), 4.20 (t, $J = 9.5$ Hz, 1H, H-2), 4.02 (d, $J = 2.8$ Hz, 1H, H-4), 3.76 (t, $J = 6.5$ Hz, 1H, H-5), 3.63 (d, $J = 6.4$ Hz, 2H, H-6a & H-6b), 3.58 (dd, $J = 9.3, 2.8$ Hz, 1H, H-3); $^{13}\text{C-NMR}$ (126 MHz, CDCl_3) δ 156.6, 149.4, 138.6, 138.3, 137.8, 136.7, 128.5, 128.4, 128.2, 128.1, 128.0, 127.8, 127.7, 127.7, 127.6, 124.4, 120.8 (each Ar-C/C-H), 85.4 (C-1), 83.6 (C-3), 78.0 (C-5), 74.6 (Bn- CH_2), 73.6 (C-4), 73.5, 72.7 (each Bn- CH_2), 70.3 (C-2), 68.6 (C-6). HRMS calcd for $\text{C}_{32}\text{H}_{33}\text{NO}_5\text{NaS}$ $[\text{M} + \text{Na}]^+$ 566.1977 found m/z 566.1959.

4.7 2-*p*-Methoxybenzyl-3,4,6-tri-*O*-benzyl- β -thiopyridine-*D*-galactopyranose (**10**)

To **9** (1.5 g, 2.76 mmol) in dry dimethylformamide (15 mL), sodium hydride (221 mg, 5.52 mmol, 60% w/w in mineral oil) was added at 0 °C. After stirring for 10 minutes, 4-meth-



oxybenzyl chloride (0.6 mL, 4.42 mmol) was added at 0 °C, and the reaction mixture was stirred at room temperature for 3 h. Ice-cold water (20 mL) was then added to the mixture and it was extracted with ethyl acetate (30 mL × 2). The organic layer was washed with water (20 mL × 2), dried over anhydrous sodium sulphate, and filtered. Removal of the solvent under reduced pressure and chromatography (silica gel, eluting with 5 : 1 cyclohexane and ethyl acetate) gave **10** (1.46 g, 80%) as a pale yellow solid; R_f 0.83 (cyclohexane–EtOAc, 1 : 1); $^1\text{H-NMR}$ (500 MHz, CDCl_3) δ 8.42 (dd, J = 5.0, 1.9 Hz, 1H), 7.47–7.21 (m, 19H), 6.99 (br t, J = 6.1 Hz, 1H), 6.80 (d, J = 8.6 Hz, 2H) (each Ar–H), 5.31 (d, J = 9.9 Hz, 1H, H-1), 5.00 (d, J = 11.4 Hz, 1H), 4.79 (d, J = 9.6 Hz, 3H), 4.73 (d, J = 9.9 Hz, 1H), 4.64 (d, J = 11.4 Hz, 1H), 4.48 (d, J = 11.7 Hz, 1H), 4.42 (d, J = 11.4 Hz, 1H) (each Bn-CH₂), 4.06 (t, J = 9.5 Hz, 1H, H-2), 4.04 (d, J = 2.6 Hz, 1H, H-4), 3.78 (s, 3H, OCH₃), 3.74 (t, J = 6.6 Hz, 1H, H-5), 3.69 (dd, J = 9.2, 2.7 Hz, 1H, H-3), 3.65 (d, J = 6.4 Hz, 2H, H-6a & H-6b); $^{13}\text{C-NMR}$ (126 MHz, CDCl_3) δ 159.2, 157.8, 149.5, 138.7, 138.4, 137.9, 136.4, 130.3, 130.1, 128.4, 128.4, 128.2, 128.1, 127.9, 127.8, 127.7, 127.6, 127.5, 123.3, 120.2, 113.7 (each Ar–C/C–H) 84.2 (C-1), 84.2 (C-3), 77.5 (C-5), 77.0 (C-2), 75.4 (Bn-CH₂), 74.6 (Bn-CH₂), 73.8 (C-4), 73.5 (Bn-CH₂), 72.8 (Bn-CH₂), 68.7 (C-6), 55.3 (OCH₃); HRMS calcd for $\text{C}_{40}\text{H}_{41}\text{NO}_6\text{NaS}$ [$\text{M} + \text{Na}$]⁺ 686.2552 found m/z 686.2539.

4.8 2-*p*-Methoxybenzyl-3,4,6-tri-*O*-benzyl- β -sulfonylpyridine-*D*-galactopyranose (**11**)

Compound **10** (1.8 g, 2.71 mmol) was dissolved in dichloromethane (30 mL), and the solution was cooled to 0 °C. Sodium bicarbonate (1.37 g, 16.3 mmol) and *m*-chloroperbenzoic acid (55–70% purity; 2.8 g) were added, and the reaction mixture was warmed to room temperature and stirred for 6 h. On completion of the reaction (TLC), the reaction mixture was diluted with dichloromethane (30 mL), and the organic layer was washed with aqueous sodium sulfite solution (30 mL × 2). The solvent was evaporated under reduced pressure, chromatography (silica gel, eluting with 4 : 1 cyclohexane and ethyl acetate) gave **11** (1.6 g, 85%) as a white solid; R_f 0.37 (cyclohexane–EtOAc 3 : 2); $^1\text{H-NMR}$ (500 MHz, CDCl_3) δ 8.62 (ddd, J = 4.8, 1.8, 0.9 Hz, 1H), 8.02 (bd, J = 7.8 Hz, 1H), 7.73 (td, J = 7.8, 1.7 Hz, 1H), 7.38–7.11 (m, 19H), 6.81 (d, J = 8.7 Hz, 2H) (each Ar–H), 4.98 (d, J = 9.6 Hz, 1H), 4.91 (d, J = 10.3 Hz, 1H) (each Bn-CH₂), 4.89 (d, J = 8.4 Hz, 1H, H-1), 4.82 (d, J = 9.7 Hz, 1H, Bn-CH₂), 4.72 (s, 2H, each Bn-CH₂), 4.55 (d, J = 7.9 Hz, 1H, H-2), 4.53 (d, J = 9.9 Hz, 2H), 4.23 (s, 2H) (each Bn-CH₂), 3.87 (d, J = 2.6 Hz, 1H, H-4), 3.79 (s, 3H, OCH₃), 3.66 (dd, J = 9.4, 2.7 Hz, 1H, H-3), 3.58 (t, J = 6.3 Hz, 1H, H-5), 3.42 (dd, J = 9.7, 6.7 Hz, 1H, H-6a), 3.37 (dd, J = 9.7, 5.8 Hz, 1H, H-6b); $^{13}\text{C-NMR}$ (126 MHz, CDCl_3) δ 159.2, 156.1, 149.9, 138.4, 138.0, 137.7, 137.3, 130.3, 130.0, 129.8, 128.5, 128.4, 128.2, 127.9, 127.5, 127.0, 123.9, 113.6 (each Ar–C/C–H), 89.5 (C-1), 83.9 (C-3), 78.2 (C-5), 74.9 (Bn-CH₂), 74.4 (Bn-CH₂), 73.9 (C-2), 73.4 (Bn-CH₂), 73.1 (C-4), 72.9 (Bn-CH₂), 68.4 (C-6), 55.3 (OCH₃); HRMS calcd for $\text{C}_{40}\text{H}_{41}\text{NO}_8\text{NaS}$ [$\text{M} + \text{Na}$]⁺ 718.2451 found m/z 718.2433.

4.9 1-((2*S*,3*R*,4*S*,5*S*,6*R*)-4,5-Bis(benzyloxy)-6-((benzyloxy)methyl)-3-((*p*-methoxybenzyl)oxy)tetrahydro-2*H*-pyran-2-yl)-2-methylpropan-1-ol (**12**)

Sulfone **11** (500 mg, 0.718 mmol) and isobutyraldehyde (0.26 mL, 2.86 mmol) were dissolved in dry tetrahydrofuran (10 mL) and cooled to 0 °C. A solution of samarium iodide in dry tetrahydrofuran (55 mL, freshly prepared sing samarium metal (1.65 g) and iodine (1.4 g)) was added at 0 °C. The resulting green coloured solution was warmed to room temperature and stirred for 20 minutes. Saturated ammonium chloride solution (30 mL) was then added and the mixture was extracted with ethyl acetate (40 mL × 2). The combined organic layer was dried over anhydrous sodium sulphate and filtered. Evaporation of the solvent under reduced pressure and subsequent chromatography (silica gel, eluting with 6 : 1 cyclohexane and ethyl acetate) gave **12** (190 mg, 42%) as a pale-yellow viscous oil, along with an impurity believe to be the 1-deoxygalactopyranose derivative. Selected data for **12** $^1\text{H-NMR}$ signals δ 3.98 (d, J = 2.7 Hz, 1H, H-4 major) HRMS calcd for $\text{C}_{41}\text{H}_{52}\text{O}_7\text{Na}$ [$\text{M} + \text{Na}$]⁺ 541.2595 found m/z 541.2566.

4.10 (2*S*,3*R*,4*R*,5*S*,6*R*)-4,5-Bis(benzyloxy)-6-((benzyloxy)methyl)-2-((*R*)-1-hydroxy-2-methylpropyl)tetrahydro-2*H*-pyran-3-ol (**13**)

To alcohol **12** (190 mg, 0.303 mmol) in dichloromethane and water (10 : 1, 2 mL) at 0 °C was added 2,3-dichloro-5,6-dicyano-1,4-benzoquinone (DDQ, 90 mg, 0.40 mmol). The reaction mixture was then stirred at room temperature for 2 h. The reaction mixture was then diluted with dichloromethane (10 mL) and washed with saturated aqueous solution of sodium bicarbonate (10 mL). The organic layer was dried with anhydrous sodium sulphate and filtered and the solvent was removed under reduced pressure. Chromatography of the residue (silica gel, eluting with 5 : 1 cyclohexane and ethyl acetate) gave **13** (93 mg, 61%) as a pale yellow oil; R_f 0.55 (cyclohexane–EtOAc 3 : 2); $^1\text{H-NMR}$ (500 MHz, CDCl_3) δ 7.43–7.21 (overlapping signals, 15H, each Ar–H), 4.88 (d, J = 11.5 Hz, 1H), 4.76 (d, J = 11.8 Hz, 1H), 4.57 (d, J = 12.2 Hz, 1H), 4.55 (d, J = 12.6 Hz, 1H), 4.50 (d, J = 11.7 Hz, 1H), 4.46 (d, J = 11.7 Hz, 1H) (each Bn-CH₂), 4.22 (t, J = 9.4 Hz, 1H, H-2), 4.01 (d, J = 2.8 Hz, 1H, H-4), 3.67–3.54 (overlapping signals, 3H, H-5, H-6a & H-6b), 3.47–3.41 (overlapping signals, 2H, H-3 & H-1'), 3.31 (bd, J = 9.4 Hz, 1H, H-1), 1.86 (h, J = 7.1 Hz, 1H, isopropyl CH), 1.02 (d, J = 6.7 Hz, 3H), 0.89 (d, J = 6.8 Hz, 3H) (each CH₃); $^{13}\text{C-NMR}$ (126 MHz, CDCl_3) δ 138.6, 137.9, 137.9, 128.6, 128.4, 128.2, 127.9, 127.9, 127.9, 127.8, 127.7, 127.6 (each Ar–C/C–H), 84.4 (C-1'), 79.0 (C-1), 77.2 (C-5), 74.5 (C-3), 74.4 (Bn-CH₂), 73.6 (Bn-CH₂), 72.8 (C-4), 71.8 (Bn-CH₂), 68.9 (C-6), 66.7 (C-2), 31.2 (C-2'), 19.3, 19.2 (each CH₃); HRMS calcd for $\text{C}_{31}\text{H}_{38}\text{O}_6\text{Na}$ [$\text{M} + \text{Na}$]⁺ 529.2566 found m/z 529.2571.

4.11 (4*S*,4*aS*,6*R*,7*S*,8*S*,8*aR*)-7,8-Bis(benzyloxy)-6-((benzyloxy)methyl)-4-isopropylhexahydropyrano[3,2-*d'*][1,3]dioxine (**14**)

Diol **13** (180 mg, 0.35 mmol) was dissolved in dimethoxy-methane (4.00 mL, 45.6 mmol), camphorsulfonic acid



(165 mg, 0.71 mmol) was added and the reaction was allowed to heat at reflux overnight while stirring vigorously. The solvent was then removed under reduced pressure and chromatography (silica gel, eluting with cyclohexane–EtOAc 6 : 1) provided **14** (110 mg, 60%) as a colourless oil; R_f 0.88 (cyclohexane–EtOAc 3 : 2); $^1\text{H-NMR}$ (500 MHz, CDCl_3) δ 7.46–7.22 (overlapping signals, 15H, each Ar–H), 4.96 (d, $J = 11.8$ Hz, 1H), 4.89–4.79 (overlapping signals, 3H), 4.71 (d, $J = 12.2$ Hz, 1H), 4.59 (d, $J = 11.7$ Hz, 1H) (each Bn-CH₂), 4.45 (s, 2H, methylene CHH & CHH), 4.21 (t, $J = 9.2$ Hz, 1H, H-2), 3.92 (d, $J = 3.0$ Hz, 1H, H-4), 3.69 (overlapping signals, 2H, H-1 & H-1'), 3.63–3.48 (overlapping signals, 4H, H-3, H-5, H-6a & H-6b), 2.42 (doublet of heptets, $J = 6.6, 2.5$ Hz, 1H, isopropyl CH), 1.03 (d, $J = 6.4$ Hz, 3H), 0.98 (d, $J = 6.5$ Hz, 3H) (each CH₃); $^{13}\text{C-NMR}$ (126 MHz, CDCl_3) δ 139.0, 138.5, 138.0, 128.5, 128.4, 128.4, 128.2, 128.1, 127.8, 127.8, 127.7, 127.7, 127.6, 127.5, 127.4 (each Ar-C/C–H), 87.9 (Bn-CH₂), 81.2 (C-3), 78.8 (C-1'), 78.0 (C-5), 76.3 (C-1), 75.1 (C-4), 74.6 (Bn-CH₂), 73.5 (methylene CH₂), 73.4 (C-2), 72.8 (Bn-CH₂), 69.1 (C-6), 25.0 (C-2'), 20.6, 19.7 (each CH₃); HRMS calcd for C₃₂H₃₈O₆Na [M + Na]⁺ 541.2566 found m/z 541.2595.

4.12 (4*S*,4*aS*,6*R*,7*S*,8*R*,8*aS*)-6-(Acetoxymethyl)-4-isopropylhexahydropyrano[3,2-*d'*][1,3]dioxine-7,8-diyl diacetate (**15**)

Compound **6** (30 mg, 0.12 mmol) was dissolved in Ac₂O (4 mL) and pyridine (4 mL) and stirred overnight. The reaction mixture was diluted with EtOAc, washed with 1 M HCl, water and brine, dried over Na₂SO₄, filtered and the solvent was removed. Chromatography (silica gel, eluting with cyclohexane–EtOAc 3 : 2) gave **15** (41 mg, 90%) as a white solid; R_f 0.41 (cyclohexane–EtOAc 3 : 2); $^1\text{H-NMR}$ (500 MHz, CDCl_3) δ 5.40 (dd, $J = 3.4, 1.3$ Hz, 1H, H-4), 5.01 (dd, $J = 9.9, 3.4$ Hz, 1H, H-3), 4.77 (d, $J = 6.5$ Hz, 1H, methylene CHH), 4.75 (d, $J = 6.4$ Hz, 1H, methylene CHH), 4.06 (dd, $J = 11.2, 6.5$ Hz, 1H, H-6a), 4.00 (dd, $J = 11.3, 6.7$ Hz, 1H, H-6b), 3.97 (d, $J = 9.7$ Hz, 1H, H-2), 3.85 (td, $J = 6.6, 1.4$ Hz, 1H, H-5), 3.78 (dd, $J = 10.0, 5.7$ Hz, 1H, H-1), 3.68 (dd, $J = 10.3, 5.7$ Hz, 1H, H-1'), 2.37 (heptet of doublets, $J = 10.1, 6.6$ Hz, 1H, isopropyl CH), 2.10 (s, 3H), 2.00 (s, 3H), 1.99 (s, 3H), 0.99 (d, $J = 6.4$ Hz, 3H), 0.96 (d, $J = 6.6$ Hz, 3H); $^{13}\text{C-NMR}$ (126 MHz, CDCl_3) δ 170.40, 170.13, 170.04 (each C=O), 87.78 (methylene CH₂), 78.29 (C-1'), 75.97 (C-1), 74.73 (C-5), 72.00 (C-3), 69.88 (C-2), 67.87 (C-4), 61.46 (C-6), 24.90 (C-2'), 20.70, 20.62, 20.57 (each OAc), 20.31, 19.47 (each CH₃).

4.13 1-((2*R*,3*R*,4*S*,5*S*,6*R*)-4,5-Bis(benzyloxy)-6-((benzyloxy)methyl)-3-((4-methoxybenzyl)oxy)tetrahydro-2*H*-pyran-2-yl)-2-methylpropan-1-one (**16**)

Alcohol **12** (750 mg, 1.2 mmol) was dissolved in CH₂Cl₂ and cooled to 0 °C. Dess–Martin Periodinane (1.14 g, 2.69 mmol) was added and the mixture stirred overnight. The reaction mixture was filtered through Celite, washed with satd. Na₂S₂O₃ solution, satd. NaHCO₃ solution, water, and brine. The organic layer was dried over MgSO₄, filtered and the solvent removed under reduced pressure. The resulting ketone product

(305 mg, 41%) was obtained after chromatography (silica gel, eluting with cyclohexane–EtOAc 6 : 1); R_f 0.66 (cyclohexane–EtOAc 6 : 1); $^1\text{H-NMR}$ (500 MHz, CDCl_3) δ 7.45–7.24 (overlapping signals, 17H), 7.18 (d, $J = 8.6$ Hz, 1H, Ar–H), 6.83 (d, $J = 8.6$ Hz, 1H, Ar–H), 4.98 (d, $J = 11.8$ Hz, 1H), 4.81–4.76 (overlapping signals, 2H), 4.73 (d, $J = 11.7$ Hz, 1H), 4.64 (d, $J = 11.7$ Hz, 1H), 4.59 (d, $J = 10.1$ Hz, 1H), 4.48 (d, $J = 11.8$ Hz, 1H), 4.44 (d, $J = 11.6$ Hz, 1H) (each Bn-CH₂), 4.18 (t, $J = 9.6$ Hz, 1H, H-2), 3.98 (d, $J = 2.8$ Hz, 1H, H-4), 3.91 (d, $J = 9.6$ Hz, 1H, H-1), 3.79 (s, 3H, OCH₃), 3.65 (dd, $J = 9.5, 2.8$ Hz, 1H, H-3), 3.63–3.56 (overlapping signals, 3H, H-5, H-6a & H-6b), 3.00 (hept, $J = 7.0$ Hz, 1H, isopropyl CH), 1.14 (d, $J = 7.0$ Hz, 3H), 1.12 (d, $J = 7.0$ Hz, 3H) (each CH₃); $^{13}\text{C-NMR}$ (126 MHz, CDCl_3) δ 209.36 (C=O), 159.24, 138.68, 138.32, 137.87, 130.55, 129.90, 129.50, 128.48, 128.47, 128.44, 128.43, 128.41, 128.34, 128.27, 128.24, 128.14, 128.02, 128.01, 127.97, 127.95, 127.89, 127.83, 127.80, 127.77, 127.69, 127.62, 127.60, 127.57, 127.55, 127.52, 127.48, 127.36, 113.82, 113.74 (each Ar-C/C–H), 84.52 (C-3), 81.01 (C-1), 77.88 (C-5), 75.39 (C-2), 74.90, 74.43, 73.57 (each Bn-CH₂), 73.51 (C-4), 72.50 (Bn-CH₂), 69.04 (C-6), 55.27 (OCH₃), 38.55 (C-2'), 18.23, 17.82 (each CH₃).

4.14 (S)-1-((2*S*,3*R*,4*S*,5*S*,6*R*)-4,5-Bis(benzyloxy)-6-((benzyloxy)methyl)-3-((4-methoxybenzyl)oxy)tetrahydro-2*H*-pyran-2-yl)-2-methylpropan-1-ol (**17**)

Ketone **16** (269 mg, 0.43 mmol) was dissolved in CH₂Cl₂–MeOH (1 : 1) and NaBH₄ (22 mg, 0.59 mmol) was added to the reaction mixture and allowed to stir for 30 min, after which TLC analysis indicated complete consumption of the starting material. The solvent was then removed under reduced pressure. Flash chromatography (cyclohexane–EtOAc 6 : 1) provided the product (230 mg, 85%) as a white solid; R_f 0.29 (cyclohexane–EtOAc 4 : 1); $^1\text{H-NMR}$ (400 MHz, CDCl_3) δ 7.44–7.15 (overlapping signals, 17H, aromatic H), 6.90–6.75 (overlapping signals, 2H, Ar–H), 5.01 (d, $J = 10.3$ Hz, 1H), 4.94 (d, $J = 11.6$ Hz, 1H), 4.78 (d, $J = 11.7$ Hz, 1H), 4.67 (d, $J = 10.4$ Hz, 1H), 4.67 (d, $J = 11.6$ Hz, 1H), 4.62 (d, $J = 11.6$ Hz, 1H), 4.48 (d, $J = 11.7$ Hz, 1H), 4.42 (d, $J = 11.6$ Hz, 1H) (each Bn-CH₂), 4.04 (t, $J = 9.4$ Hz, 1H, H-2), 3.99 (d, $J = 2.7$ Hz, 1H, H-4), 3.78 (s, 3H, OCH₃), 3.68 (dd, $J = 9.4, 2.7$ Hz, 1H, H-3), 3.64 (dd, $J = 6.7, 3.7$ Hz, 1H, H-1'), 3.55 (s, 3H, H-5, H-6a & H-6b), 3.23 (dd, $J = 9.2, 6.8$ Hz, 1H, H-1), 2.02 (tdd, $J = 10.5, 5.2, 2.6$ Hz, 1H, isopropyl CH), 0.95 (d, $J = 7.0$ Hz, 3H), 0.87 (d, $J = 6.8$ Hz, 3H) (each CH₃); $^{13}\text{C-NMR}$ (101 MHz, CDCl_3) δ 130.02, 129.93, 128.65, 128.55, 128.37, 128.19, 127.97, 127.92, 127.89, 127.74, 127.69, 114.03 (each aromatic C/C–H), 85.49 (C-3), 78.72 (C-1), 78.48 (C-2), 77.54 (C-1'), 77.51 (C-5), 75.08, 74.65, 73.63 (each Bn-CH₂), 73.61 (C-4), 72.19 (Bn-CH₂), 69.08 (C-6), 55.38 (OCH₃), 28.83 (C-2'), 19.66, 15.64 (each CH₃); HRMS calcd for C₄₁H₅₂O₇Na [M + Na]⁺ 649.3136 found m/z 649.3134.

4.15 (4*S*,4*aS*,6*R*,7*S*,8*S*,8*aR*)-7,8-Bis(benzyloxy)-6-((benzyloxy)methyl)-4-isopropylhexahydropyrano[3,2-*d'*][1,3]dioxine (**18**)

Alcohol **17** (200 mg, 0.32 mmol) was dissolved in CH₂Cl₂ and cooled to 0 °C. Trifluoroacetic acid (0.32 mL, 4.23 mmol) was added to the reaction mixture and allowed to stir for 30 min,



after which time TLC analysis indicated complete consumption of the starting material. The solvent was then removed under reduced pressure and chromatography (cyclohexane–EtOAc 4 : 1) provided the intermediate diol (126 mg, 78%) as a white solid; R_f 0.3 (cyclohexane–EtOAc 3 : 2); $^1\text{H-NMR}$ (500 MHz, CDCl_3) δ 7.41–7.24 (overlapping signals, 15H, each Ar–H) 4.86 (d, $J = 11.6$ Hz, 1H), 4.74 (d, $J = 11.7$ Hz, 1H), 4.62 (d, $J = 11.6$ Hz, 1H), 4.56 (d, $J = 11.8$ Hz, 1H), 4.50 (d, $J = 11.7$ Hz, 1H), 4.45 (d, $J = 11.8$ Hz, 1H) (each Bn-CH₂), 4.13 (t, $J = 9.3$ Hz, 1H, H-2), 3.99 (d, $J = 2.8$ Hz, 1H, H-4), 3.72 (dd, $J = 7.7, 3.1$ Hz, 1H, H-1'), 3.61 (dd, $J = 12.4, 5.4$ Hz, 1H, H-5), 3.57–3.53 (overlapping signals, 2H, H-6a & H-6b) 3.46 (dd, $J = 9.4, 2.9$ Hz, 1H, H-3), 3.19 (dd, $J = 9.1, 7.6$ Hz, 1H, H-1), 2.09 (pd, $J = 6.9, 3.1$ Hz, 1H, isopropyl CH), 0.98 (d, $J = 7.0$ Hz, 3H), 0.89 (d, $J = 6.8$ Hz, 3H) (each CH₃); $^{13}\text{C-NMR}$ (126 MHz, CDCl_3) δ 138.47, 137.91, 137.87, 128.64, 128.60, 128.44, 128.27, 128.18, 127.96, 127.87, 127.82, 127.76, 127.67, 113.96 (each Ar–C/C–H), 83.86 (C-3), 78.29 (C-1), 78.27 (C-1'), 77.42 (C-5), 74.46, 73.55 (each Bn-CH₂), 72.69 (C-4), 72.02 (Bn-CH₂), 71.61 (C-2), 68.96 (C-6), 28.74 (C-2'), 19.30, 15.02 (each CH₃); HRMS calcd for $\text{C}_{32}\text{H}_{41}\text{O}_6\text{Na}$ [$\text{M} + \text{Na}$]⁺ 529.2560 found m/z 529.2563. The intermediate (126 mg, 0.25 mmol) was dissolved in dimethoxy-methane (4.00 mL, 45.6 mmol), camphorsulfonic acid (115 mg, 0.49 mmol) was added and the mixture was heated at reflux for 18 h while stirring vigorously. The solvent was removed under reduced pressure and flash chromatography (cyclohexane–EtOAc 6 : 1) provided **18** (81 mg, 63%) as a colourless oil; R_f 0.88 (cyclohexane–EtOAc 3 : 2); $^1\text{H-NMR}$ (500 MHz, CDCl_3) δ 7.44–7.23 (overlapping signals, 15H, Ar–H), 5.13 (d, $J = 6.2$ Hz, 1H, methylene CHH), 4.96 (d, $J = 11.4$ Hz, 1H), 4.84 (d, $J = 12.2$ Hz, 1H) (each Bn-CH₂), 4.77 (d, $J = 6.3$ Hz, 1H, methylene CHH), 4.71 (d, $J = 12.3$ Hz, 1H), 4.63 (d, $J = 11.4$ Hz, 1H), 4.47 (d, $J = 11.8$ Hz, 1H), 4.42 (d, $J = 11.8$ Hz, 1H) (each Bn-CH₂), 4.00–3.93 (overlapping signals, 2H, H-2 & H-4), 3.65 (dd, $J = 9.8, 3.0$ Hz, 1H, H-3), 3.61 (dd, $J = 12.4, 5.4$ Hz, 1H, H-5), 3.57–3.53 (overlapping signals, 2H, H-6a & H-6b), 3.44 (dd, $J = 9.3, 2.9$ Hz, 1H, H-1'), 3.12 (t, $J = 9.2, 9.1$ Hz, 1H, H-1), 2.05 (pd, $J = 7.0, 2.8$ Hz, 1H, isopropyl CH), 1.00 (d, $J = 7.0$ Hz, 3H), 0.93 (d, $J = 6.8$ Hz, 3H) (each CH₃); $^{13}\text{C-NMR}$ (126 MHz, CDCl_3) δ 138.47, 137.93, 128.50, 128.42, 128.23, 127.85, 127.78, 127.67, 127.59, 127.53 (each Ar–C or Ar C–H), 93.82 (methylene CH₂), 82.50 (C-1'), 80.51 (C-3), 78.59 (C-2), 78.30 (C-5), 74.99 (Bn-CH₂), 74.88 (C-4), 74.26 (C-1), 73.52, 72.81 (each Bn-CH₂), 68.87 (C-6), 27.99 (C-2'), 19.11, 15.71 (each CH₃).

4.16 Measurements of galactosidase inhibition

Each galactosidase assay was performed according to a procedure previously described by Bols *et al.* preparing eight 250 μL samples in cuvettes containing 100 μL of either sodium phosphate buffer (0.1 M) containing 10 mM MgCl_2 and 1 mg mL^{-1} BSA of pH 6.5, or sodium acetate buffer (0.1 M) containing 1 mg mL^{-1} BSA of pH 4.5, along with 10 to 80 μL of a 5 or 10 mM solution of either 4-nitrophenyl α -D-galactopyranoside or 4-nitrophenyl β -D-galactopyranoside in water, and 20 μL of a solution of either the potential inhibitor (**1–6**) or water, and

topped up to a total volume of 250 μL with distilled water. All the test samples were made up to 230 μL , containing the potential inhibitor at a fixed concentration but with varying concentrations of nitrophenyl glycoside. The control samples were made up to 250 μL , they contained no inhibitor, but also varying concentrations of the nitrophenyl glycoside. Finally, the reaction was started by adding 20 μL of a diluted solution of either β -galactosidase from *E. coli* (EC 3.2.1.23, Megazyme E-ECBGAL), β -galactosidase from *A. niger* (EC 3.2.1.23, Megazyme E-BGLAN) or α -galactosidase from *A. niger* (EC 3.2.1.22, Megazyme E-AGLAN). The formation of 4-nitrophenol was monitored for 2–10 min at 26 °C by measurement of the absorbance at 400 nm. Initial velocities were calculated from the slopes for each of the eight reactions and used to construct two Hanes plots, one with and one without inhibitor. From the two Michaelis–Menten constants (K_m) thus obtained, the inhibition constant (K_i) was calculated.

4.17 Computational methods

4.17.1 Protein preparation and ligand preparation for computations. The crystal structure providing atomic details of IPTG **1** bound to the lac repressor at 2.0 Å resolution was downloaded from the protein databank (PDB ID = 2P9H).⁴⁷ These coordinates were subjected to the protein preparation workflow in Maestro as described previously,⁴⁸ which involved assigning bond orders, replacement of hydrogen atoms and generation of protonation states (pH = 7.4), followed by optimization of H-bonding interactions, energy minimization including the removal of any crystallized water molecules at more than 5 Å distance from the ligands. The resulting coordinates were used for docking MMGBSA and dynamics studies and these are provided with the ESI.† The ligands were built in Maestro and the starting three-dimensional (3D) coordinates were generated for all ligands with LigPrep,⁴⁹ which generates low energy conformations.

4.17.2 Conformational analysis of ligands. Low energy geometries generated using ligprep where the galactopyranose derivative had $^4\text{C}_1$ chair were starting point for metadynamics. Conformational analysis was performed for **1–6** using Desmond metadynamics simulations again implemented in Maestro using OPLS4 force field. For the metadynamics the ligands were subjected to buffer box size calculation method, using the Desmond system builder, to generate an orthorhombic box of SP3 water molecules prepared for metadynamics. For the metadynamics the current variables (CVs) selected were ϕ and ψ with up to 1000 structures generated in up to 10 ns simulations, which corresponds to one structure sampled every 0.01 ns. The energy surface plots were subsequently generated using the metadynamics analysis tool in Maestro from the trajectory generated. The coordinates for lowest energy structure from each of the plots for **1–6** are given in the ESI.†

4.17.3 Docking and MM-GBSA calculations. The docking receptor grid was generated using the protein–ligand coordinates, based on IPTG binding at one of the ligand sites (site A) and contained water molecules within 5 Å distance from IPTG



as obtained from the protein preparation protocol. The docking receptor grid was generated with the default settings in Glide using the co-crystallized ligand to define the centre of the box; a default van der Waals scaling factor of 1.0 was chosen for non polar parts of the receptor with a partial charge cutoff of 0.25; no constraints, excluded volumes or rotatable groups were selected. The ligand structures for docking were pre-prepared using the ligprep module. For docking, flexible ligand sampling was allowed with a final minimization of docked poses performed. A default van der Waals scaling factor of 0.8 was applied to non-polar atoms of the ligands with a partial charge cutoff of 0.15. No constraints were applied apart from the rigid receptor, with up to five poses being generated for each ligand. The binding pose generated after docking of IPTG was in good agreement with the structure in the co-crystal structure (RMSD 1.88 Å). The poses obtained from docking were used for MMGBSA calculations with Prime MM-GBSA as implemented in Maestro; the default parameters were used with the VSGB solvation module selected.

4.17.4 Binding pose metadynamics and 100 ns molecular dynamics. The protocol for Desmond binding pose metadynamics (BPMD) was implemented in Maestro. Before the simulation, the protein and ligand coordinates obtained from the Prime protein preparation workflow were placed in an orthorhombic box of SPC water molecules, using the Desmond system builder, with a buffer of 10 Å between the solute structures and the simulation box boundary on each axis, choosing the OPLS4 forcefield. The IPTG 1 in site A was subjected to 10 trials of BPMD, with each trial subjected to 10 ns molecular dynamics, with 50 structures sampled for each trial. The output files and trajectories from each trial were subsequently analysed in addition to the reports generated by Desmond. For molecular dynamics the ligand protein complexes were similarly prepared and subjected to 100 ns simulations in Desmond and the Desmond MD analysis tool used to generate the reports for each ligand. These detailed reports are provided as ESI.† The trajectories were also analysed as described in the text above.

Data availability

The data supporting this article have been included as part of the ESI.†

Conflicts of interest

There are no conflicts of to declare.

Acknowledgements

Research presented herein was financially supported by Science Foundation Ireland (Grant No. 16/IA/4419). SA obtained an Erasmus+ mobility fellowship. PVM acknowledges

the Irish Centre for High-End Computing (ICHEC) for the provision of computational facilities and support. The authors thank Andrew Flaus for providing the pET28-eGFP vector Daniel Pritko and Marc R Birtwistle for providing the vector pQLinkHD-mTFP1.

References

- H. Yuasa and H. Hashimoto, *Trends Glycosci. Glycotechnol.*, 2001, **13**, 31–55.
- (a) P. G. Goekjian, T. C. Wu and Y. Kishi, *J. Org. Chem.*, 1991, **56**, 6412–6422; (b) V. García-Aparicio, M. Sollogoub, Y. Blériot, V. Colliou, S. André, J. L. Asensio, F. J. Cañada, H. J. Gabius, P. Sinay and J. Jiménez-Barbero, *Carbohydr. Res.*, 2007, **342**, 1918–1928.
- (a) F. Strino, J. H. Lii, H. J. Gabius and P. G. Nyholm, *J. Comput.-Aided Mol. Des.*, 2009, **23**, 845–852; (b) E. Montero, A. García-Herrero, J. L. Asensio, K. Hirai, S. Ogawa, F. Santoyo-González, F. J. Cañada and J. Jiménez-Barbero, *Eur. J. Org. Chem.*, 2000, 1945–1952.
- L. M. Mikkelsen, M. J. Hernáiz, M. Martín-Pastor, T. Skrydstrup and J. Jiménez-Barbero, *J. Am. Chem. Soc.*, 2002, **124**, 14940–14951.
- (a) R. U. Lemieux, A. A. Pavia, J. C. Martin and K. A. Watanab, *Can. J. Chem.*, 1969, **47**, 4427; (b) I. Tvaroška and T. Bleha, *Anomeric and Exo-Anomeric Effects in Carbohydrate Chemistry*, ed. R. S. Tipson and D. Horton, *Advances in Carbohydrate Chemistry and Biochemistry*, Academic Press, 1989, vol. 47, pp. 45–123.
- T. C. Wu, P. G. Goekjian and Y. Kishi, *J. Org. Chem.*, 1987, **52**, 4819–4823.
- (a) J. F. Espinosa, F. J. Cañada, J. L. Asensio, M. Martín-Pastor, H. Dietrich, R. R. Schmidt and J. Jiménez-Barbero, *J. Am. Chem. Soc.*, 1996, **118**, 10862–10871; (b) M. Martín-Pastor, A. Canales, F. Corzana, J. L. Asensio and J. Jiménez-Barbero, *J. Am. Chem. Soc.*, 2005, **127**, 3589–3595.
- R. Sommer, K. Rox, S. Wagner, D. Hauck, S. S. Henrikus, S. Newsad, T. Arnold, T. Ryckmans, M. Brönstrup, A. Imberty, A. Varrot, R. W. Hartmann and A. Titz, *J. Med. Chem.*, 2019, **62**, 9201–9216.
- I. L. Quintana, A. Paul, A. Chowdhury, K. D. Moulton, S. S. Kulkarni and D. H. Dube, *ACS Infect. Dis.*, 2023, **9**, 2025–2035.
- F. Stauffert, A. Bodlenner, T. M. N. Trinh, M. I. García-Moreno, C. O. Mellet, J. F. Nierengarten and P. Compain, *New J. Chem.*, 2016, **40**, 7421–7430.
- A. Marbach and K. Bettenbrock, *J. Biotechnol.*, 2012, **157**, 82–88.
- M. Lewis, G. Chang, N. C. Horton, M. A. Kercher, H. C. Pace, M. A. Schumacher, R. G. Brennan and P. Lu, *Science*, 1996, **271**, 1247–1254.
- (a) B. Müller-Hill, H. V. Rickenberg and K. Wallenfels, *J. Mol. Biol.*, 1964, **10**, 303–318; (b) M. D. Barkley, A. D. Riggs, A. Jobe and S. Bourgeois, *Biochemistry*, 1975, **14**, 1700–1712.



- 14 R. Daber, S. Stayrook, A. Rosenberg and M. Lewis, *J. Mol. Biol.*, 2007, **370**, 609–619.
- 15 In ref. 16 2 is referred to as IBCG, abbreviated from 'isobutyl C-galactoside' although the latter is not an IUPAC name.
- 16 K. S. Ko, J. Kruse and N. Pohl, *Org. Lett.*, 2003, **5**, 1781–1783.
- 17 C. P. Sager, B. Fiege, P. Zihlmann, R. Vannam, S. Rabbani, R. P. Jakob, R. C. Preston, A. Zalewski, T. Maier, M. W. Peczuh and B. Ernst, *Chem. Sci.*, 2018, **9**, 646–654.
- 18 R. Caraballo, M. Sakulsombat and O. Ramström, *ChemBioChem*, 2010, **11**, 1600–1606.
- 19 Y. Yang and B. Yu, *Chem. Rev.*, 2017, **117**, 12281–12356.
- 20 N. Miquel, G. Doisneau and J. M. Beau, *Angew. Chem., Int. Ed.*, 2000, **39**, 4111–4114.
- 21 W. Adam, J. Bialas and L. Hadjarapoglou, *Chem. Ber.*, 1991, **124**, 2377.
- 22 C. H. Marzabadi and C. D. Spilling, *J. Org. Chem.*, 1993, **58**, 3761–3766.
- 23 (a) M. Szostak, M. Spain and D. J. Procter, *J. Org. Chem.*, 2012, **77**, 3049–3059; (b) C. Beemelmans and H. U. Reissig, *Angew. Chem., Int. Ed.*, 2010, **49**, 8021–8025.
- 24 H. Ando, S. Manabe, Y. Nakahara and Y. Ito, *Angew. Chem., Int. Ed.*, 2001, **40**, 4725–4728.
- 25 G. Veeresa and A. Datta, *Tetrahedron Lett.*, 1998, **39**, 3069–3070.
- 26 L. Liu, B. A. Motaal, M. Schmidt-Supprian and N. L. B. Pohl, *J. Org. Chem.*, 2012, **77**, 1539–1546.
- 27 M. Karplus, *J. Am. Chem. Soc.*, 1963, **85**, 2870–2871.
- 28 F. Mohamadi, N. G. J. Richards, W. C. Guida, R. Liskamp, M. Lipton, C. Caufield, G. Chang, T. Hendrickson and W. C. Still, *J. Comput. Chem.*, 1990, **11**, 440–467.
- 29 C. Lu, C. Wu, D. Ghoreishi, W. Chen, L. Wang, W. Damm, G. A. Ross, M. K. Dahlgren, E. Russell, C. D. V. Bargaen, R. Abel, R. A. Friesner and E. D. Harder, *J. Chem. Theory Comput.*, 2021, **17**, 4291–4300.
- 30 K. J. Bowers, E. Chow, H. Xu, R. O. Dror, M. P. Eastwood, B. A. Gregersen, J. L. Klepeis, I. Kolossvary, M. A. Moraes, F. D. Sacerdoti, J. K. Salmon, Y. Shan and D. E. Shaw, Proceedings of the ACM/IEEE Conference on Supercomputing (SC06), Tampa, Florida, 2006, November 11–17 (DOI: [10.1109/SC.2006.54](https://doi.org/10.1109/SC.2006.54)).
- 31 *Schrödinger Release 2023-4 Maestro version 13.8.135*, Schrödinger, LLC, New York, NY, 2024.
- 32 P. M. Matias and G. A. Jeffrey, *Carbohydr. Res.*, 1986, **153**, 217–226.
- 33 K. N. Kirschner and R. J. Woods, *Proc. Natl. Acad. Sci. U. S. A.*, 2001, **98**, 10541–10545.
- 34 (a) H. Y. Holzapfel, A. D. Stern, M. Bouhaddou, C. M. Anglin, D. Putur, S. Comer and M. R. Birtwistle, *ACS Comb. Sci.*, 2018, **20**, 653–659; (b) K. Weisshart, P. Pestryakov, R. W. P. Smith, H. Hartmann, E. Kremmer, O. Lavrik and H. P. Nasheuer, *J. Biol. Chem.*, 2004, **279**, 35368–35376.
- 35 H. P. Nasheuer and F. Grosse, *J. Biol. Chem.*, 1988, **263**, 8981–8988.
- 36 P. Dvorak, L. Chrast, P. I. Nikel, R. Fedr, K. Soucek, M. Sedlackova, R. Chaloupkova, V. de Lorenzo, Z. Prokop and J. Damborsky, *Microb. Cell Fact.*, 2015, **14**, 201–215.
- 37 R. Daber, S. Stayrook, A. Rosenberg and M. Lewis, *J. Mol. Biol.*, 2007, **370**, 609–619.
- 38 (a) M. Tamres, *J. Am. Chem. Soc.*, 1952, **74**, 3375–3378; (b) M. Nishio, *Phys. Chem. Chem. Phys.*, 2011, **13**, 13873–13900.
- 39 R. A. Friesner, J. L. Banks, R. B. Murphy, T. A. Halgren, J. J. Klicic, D. T. Mainz, M. P. Repasky, E. H. Knoll, M. Shelley, J. K. Perry, D. E. Shaw, P. Francis and P. S. Shenkin, *J. Med. Chem.*, 2004, **47**, 1739–1749.
- 40 G. Rastelli, A. D. Rio, G. Degliesposti and M. Sgobba, *J. Comput. Chem.*, 2010, **31**, 797–810.
- 41 A. J. Clark, P. Tiwary, K. Borrelli, S. Feng, E. B. Miller, R. Abel, R. A. Friesner and B. J. Berne, *J. Chem. Theory Comput.*, 2016, **12**, 2990–2998.
- 42 M. Bols, R. G. Hazell and I. B. Thomsen, *Chem. – Eur. J.*, 1997, **3**, 940–947.
- 43 M. L. Dugdale, D. L. Dymianiw, B. K. Minhas, I. D. Angelo and R. E. Huber, *Biochem. Cell Biol.*, 2010, **88**, 861–869.
- 44 A. Biela-Banaś, F. Oulaïdi, S. Front, E. Gallienne, K. Ikeda-Obatake, N. Asano, D. A. Wenger and O. R. Martin, *ChemMedChem*, 2014, **9**, 2647–2652.
- 45 D. H. Juers, T. D. Heightman, A. Vasella, J. D. McCarter, L. Mackenzie, S. G. Withers and B. W. Matthews, *Biochemistry*, 2001, **40**, 14781–14794.
- 46 P. Cheshev, A. Marra and A. Dondoni, *Carbohydr. Res.*, 2006, **341**, 2714–2716.
- 47 H. M. Berman, J. Westbrook, Z. Feng, G. Gilliland, T. N. Bhat, H. Weissig, I. N. Shindyalov and P. E. Bourne, The Protein Data Bank, *Nucleic Acids Res.*, 2000, **28**, 235–242.
- 48 G. M. Sastry, M. Adzhigirey, T. Day, R. Annabhimoju and W. Sherman, Protein and ligand preparation: Parameters, protocols, and influence on virtual screening enrichments, *J. Comput.-Aided Mol. Des.*, 2013, **27**, 221–234.
- 49 *Schrödinger Release 2024-2: LigPrep*, Schrödinger, LLC, New York, NY, 2024.

